Measurement of Thermal Diffusivity of a Nuclear Fuel Rod by Thermal Wave Method Based on Green Function

by

Jingbo Xiang

Bachelor of Science in Thermal Science and Energy Engineering, University of Science and Technology of China, 2017

Submitted to the Graduate Faculty of the

Swanson School of Engineering in partial fulfillment

of the requirements for the degree of

Master of Science in Mechanical Engineering

University of Pittsburgh

2020

UNIVERSITY OF PITTSBURGH

SWANSON SCHOOL OF ENGINEERING

This thesis was presented

by

Jingbo Xiang

It was defended on

April 3, 2020

and approved by

Heng Ban, Ph.D., Professor, Department of Mechanical Engineering and Materials Science

Qingming Wang, Ph.D., Professor, Department of Mechanical Engineering and Materials Science

Giovanni Paolo Galdi, Ph.D., Professor, Department of Mechanical Engineering and Materials Science

Thesis Advisor: Heng Ban, Ph.D., Professor, Department of Mechanical Engineering and Materials Science

Measurement of Thermal Diffusivity of a Nuclear Fuel Rod by Thermal Wave Method Based on Green Function

Jingbo Xiang, MS

University of Pittsburgh, 2020

The knowledge of thermal property change of nuclear fuel as a function of fuel burnup is essential for the design, operation and safety of nuclear power plants. However, there is a critical data gap in metallic fuels for advanced reactors. Ideally, fuel thermal property is measured in a reactor to reflect the neutronics heating and irradiation environment. In the thesis, a method of measuring thermal diffusivity of a nuclear fuel rod by thermal wave method based on Green function is developed and a related lab test experiment is also developed. This measurement method focuses on a surrogate fuel-heat sink couple using Joule-heating generated fuel layer, which is contained in heat sink, without breaking the container of the fuel. In addition, in the test experiment, a plate model has been used to simulate nuclear fuel rods, based on the same 1D heat transfer theory, with controllable thermal contact. AC current is applied to generate heat in the fuel layer and an IR video camera is used to measure the phase difference of temperature change between fuel layer and heat sink. The sample design is based on the sensitivity analysis result. In the experiment, the control of thermal contact resistance between fuel layer is proven to be important to the measurement. The theoretical work and computational simulation provided measurement sensitivity maps to optimize the experiment design and the experimental data showed, if the thermal resistance is controlled or minimized, the novel measurement method can be used in a reactor with further design optimizations.

Table of Contents

List of Tables

List of Figures

1.0 Introduction

1.1 Background

Fuel thermal properties are essential for fuel performance assessment including safety analysis and validation of lower length scale computational models. For metal fuels, for instance, fuel thermal conductivity largely determines power-to-melt ratio and, during normal operation, the peak fuel operating temperature. It is well known that a commercial ceramic fuel pellet undergoes significant compositional and structural changes that vary radially, and the temperature distribution across the fuel radius can be on the order of 1000 ◦C as it is being used in a light water reactor. [1]For safer and more efficient fuel design, thermal transport properties of fuels at microscales are needed to better describe the microstructure-property relationship and to validate multiscale, multi-physics computational tools.

With increased interest in metallic fuels from the advanced fuels research for next generation reactors, and especially the effort on metal fuels, it is essential to have thermal conductivity data for irradiated fuels at different burnups to assess fuel performance and safety margins. [2]However, the only available data for irradiated U-Pu-Zr fuels are from a single paper published in 1990s based on the work performed for the Integral Fast Reactor program in 1980s. In that paper, thermal conductivity estimates were made on four irradiated metallic fuel pins of relatively low burnup (one U-10Zr pin from M7, 2.9 at.% burnup; and three U-19Pu-10Zr pins from M5, 0.8 at.% and 1.9 at.% burnup and from M6, 1.9 at.% burnup) from power-to-melt the transient reactor experiments. As U-Pu-Zr fuels are considered as primary driver fuels for a new test reactor to be built in the United States, it is crucial to understand the thermal conductivity of

these fuels. However, there is a critical knowledge gap in irradiated U-Pu-Zr fuel thermal conductivity.

There are a huge number of methods for thermal properties measuring method for solid material, such as [3]photothermal technique, [4]flash method, [5]transient hot wire method, [6]transient torque method, etc. All of them rely on using a sample in the lab for measurement, which is difficult to achieve with nuclear fuels due to their intense radioactivity. The sample preparation and measurement must be performed in a radioactive hot cell, and there are very few places in the world which have such capability. [7]To truly reflect the fuel property changes in reactor operation, measurements should ideally be performed in-reactor with neutronic heating. The transient reactor at the Idaho National Laboratory can be used for such an experiment because its reactivity can be programmed to follow a specific curve. A sinusoidal heating as a function of time can allow thermal property measurement using the thermal wave method.

1.2 Thermal Wave Method and Green Function

Thermal wave is a temperature oscillation inside the sample that is excited by a periodic heat source. The propagation of thermal wave is dependent on the thermal diffusivity of the medium. The amplitude and/or phase of thermal wave with or without spatial offset from the initial thermal wave generation source can be used to measure thermal transport properties, such as thermal diffusivity or thermal conductivity. [8]The thermal wave concept describes the temporal and spatial propagation of a temperature under modulated heating. Nowadays, [9]thermal-wave physics is playing an ever-increasing role in the study of material parameters. For example, thermal-wave imaging of subsurface features has been performed with [10]gas-microphone

photoacoustics, [11]photothermal techniques, and [12]piezoelectric photoacoustics. It can be also used for [13]flaw detection in metal, [14]measurement of pyroelectric current spectrum, [15]thermal diffusivity an conductivity, and so on.

In the theoretical description of thermal waves, Green function is often used as a tool in the mathematical derivation. [16]A Green function is an integral kernel that can be used to solve differential equations from a large number of families including simpler examples such as ordinary differential equations with initial or boundary value conditions, as well as more difficult examples such as inhomogeneous partial differential equations (PDE) with boundary conditions. [17]Many-body Green Function (GF) techniques are powerful methods for addressing problems where strong correlation and excited states dictate key properties of chemical and material systems. Traditionally, Green Function is used to solve [18]molecular systems, [19]properties of amorphous and disordered materials, etc. For the measurement of thermal properties of nuclear fuel rod model, it is also applicable since it's multiple layers problem.

1.3 Goal and Objectives

This study aims to provide proof-of-concept testing for in situ measurement of thermal diffusivity/conductivity in transient nuclear reactor using thermal wave method. Specific objectives include:

Design a measurement method based on thermal wave method for 1D 3 layers self-heated solid fuel material without direct probe connection to the fuel.

Perform sensitivity analysis based on a theoretical model to identify major uncertainty sources and to predict measurement uncertainty.

Build and conduct lab experiments to validate the application of thermal wave method to surrogate fuel materials using Joule-Heating to generate thermal wave.

2.0 Theory and Modeling

For nuclear fuel experiment for property measurement in a reactor, the conceptual model of it can be simplified as concentric cylinders shown in Figure 1. The body part of this structure is a 3-layer cylinder, which includes the red part as fuel, grey part as cladding and green part as a heat sink in Figure 1. The test vessel is irrelevant for the thermal wave transient and the heating element outside the test vessel is for heating the whole test system to a reference temperature. After assuming the fuel layer is homogeneously self-heated, the heat transfer model of this 3-layer cylinder is a 1D heat transfer along the radius of the cylinder. In the lab proof-of-concept experiment, due to the difficulty of making a 3-layer concentric cylinder, 1D heat transfer model will be applied to the 3-layer semi-infinite plate model, with the boundary condition of the exposed surface of fuel layer is insulation condition. For these reasons, the theory of the measurement method is based on this 3-layer semi-infinite plate model with insulation boundary condition on the exposed surface of fuel layer. The length of the plate is infinite, but the thickness and width of the plate are finite.

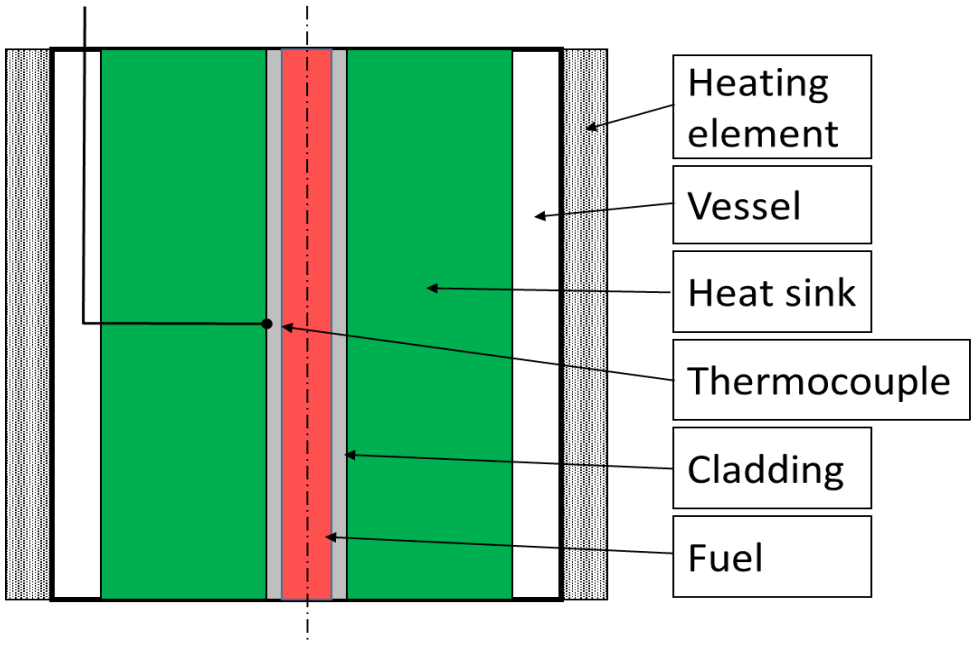

Figure 1. Simplify model of nuclear fuel rod

2.1 1D Formulation

The 1D 3-layer plate heat transfer model is shown as Figure 2. X is the direction of heat conduction. The exposed surface of fuel layer is insulated. The length of each layer is infinite. Because the fuel layer is homogeneously self-heated, the temperature of each plane along x direction is homogeneous.

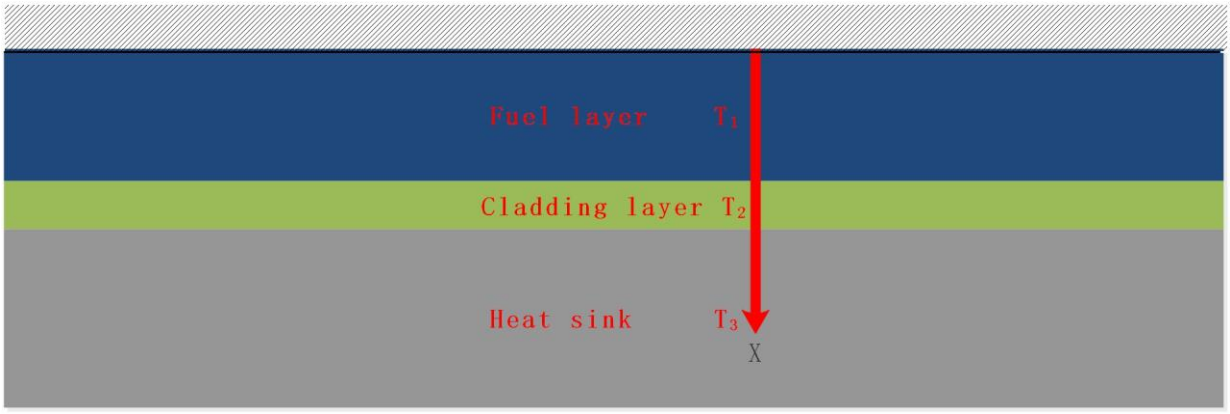

Figure 2. 1D 3-layer plate heat transfer model

Assuming the thickness of each layer of the plate is equal to δ_i. Thermal homogeneous materials are assumed for each layer. A single layer is confined in the region X_i and X_{i+1}, with $X_i = \delta_1 + \delta_2 + \cdots + \delta_i,\ i = 1, 2, 3$. Since heat generation only occurs in first layer, the governing equations for heat transport in the plate across total 3 layers are given by

$$\frac{\partial}{\partial x}\left[\frac{\partial T_i(x,t)}{\partial x}\right] = \frac{1}{\alpha_i}\frac{\partial T_i(x,t)}{\partial t} - \frac{g_i(x,t)}{k_i}\delta_{i1}\,, \delta_{i1} = \begin{bmatrix}1, i = 1\\ 0, i \neq 1\end{bmatrix} \tag{2-1}$$

where T is temperature along the *x* direction at time *t*, α thermal diffusivity, and *k* thermal conductivity. Eq. (2-1) is subjected to the following BCs and IC,

$$k_i\frac{\partial T_i(X_i,t)}{\partial x} = k_{i+1}\frac{\partial T_{i+1}(X_i,t)}{\partial x} \tag{2-2}$$

$$\frac{\partial T_1(0,t)}{\partial x} = 0 \tag{2-3a}$$

$$T_3(X_3,t) = T_0 \tag{2-3b}$$

$$T_i(x,0) = T_0 \tag{2-4}$$

The continuity conditions are assumed at the interfaces between any layers. The outer surface at $x = X_3$ maintains constant temperature, i.e., Dirichlet boundary condition.

When heat generation is modulated at frequency *f*, such as $g_i(x,t) = \text{Real}[\tilde{g}_i(x,\omega)exp\,(j\omega t)]$ where angular frequency $\omega = 2\pi f$, the resulting temperature field is

also modulated at the same frequency, yielding $T_i(x,t) - T_0 = \text{Real}[\tilde{T}_i(x,\omega)exp\ (j\omega t)]$. Eqs. (2-1) -(2-3) can be rewritten in frequency domain as

$$\frac{\partial}{\partial x}\left[\frac{\partial \tilde{T}_i(x,\omega)}{\partial x}\right] - \sigma_i^2 \tilde{T}_i(x,\omega) = -\frac{\delta_{i1}}{k_i}\tilde{g}_i(x,\omega) \tag{2-5}$$

$$k_i \frac{\partial \tilde{T}_i(X_i,\omega)}{\partial x} = k_{i+1}\frac{\partial \tilde{T}_{i+1}(X_i,\omega)}{\partial x} \tag{2-6}$$

$$\frac{\partial \tilde{T}_1(0,\omega)}{\partial x} = 0 \tag{2-7a}$$

$$\tilde{T}_3(X_3,\omega) = 0 \tag{2-7b}$$

With the introduction of Green function which represents temperature at the probe point *x* in response to the heating spot x', Eqs. (2-5) -(2-7) are rewritten as

$$\frac{d}{dx}\left[\frac{dG_i(x,\omega)}{dx}\right] - \sigma_i^2 G_i(x,\omega) = -\frac{\delta_{i1}}{\alpha_i}\delta(x-x') \tag{2-8}$$

$$k_i \frac{dG_i(X_i,\omega)}{dx} = k_{i+1}\frac{dG_{i+1}(X_i,\omega)}{dx} \tag{2-9}$$

$$\frac{dG_1(0,\omega)}{dx} = 0 \tag{2-10a}$$

$$G_3(X_3,\omega) = 0 \tag{2-10b}$$

with $\tilde{T}_i(x,\omega) = \sum_{j=1}^{N}\frac{\alpha_j}{k_j}\int_{X_{j-1}}^{X_j}\tilde{g}(x',\omega)G_i(x|x';\omega)dx'$ and $\sigma_i \equiv \sqrt{\frac{i\omega}{\alpha_i}}$ the complex wave number. As heat is applied at x' in the *first* layer $0 \le x' \le X_1$, the Green function has a solution in the following form,

$$G_1(x|x') = \begin{cases} A_{1-}I_0(\sigma_1 x) + B_{1-}K_0(\sigma_1 x), 0 \le x \le x' \\ A_{1+}I_0(\sigma_1 x) + B_{1+}K_0(\sigma_1 x), x' \le x \le X_1 \end{cases} \tag{2-11a}$$

$$G_i(x|x') = A_i I_0(\sigma_i x) + B_i K_0(\sigma_i x), \qquad x > X_1 \tag{2-11b}$$

Integrate Eq. (2-11a), we obtain the following conditions at the discontinuity,

$$\frac{d}{dx}G_1(x|x';\omega)|_{x=x'_+} - \frac{d}{dx}G_1(x|x';\omega)|_{x=x'_-} = -\frac{1}{\alpha_1 x'} \tag{2-12a}$$

$$G_1(x|x';\omega)|_{x=x'_+} = G_1(x|x';\omega)|_{x=x'_-} \tag{2-12b}$$

The constants in Eq. (2-11) can be determined by substitute Eq. (2-11) into Eqs. (2-9), (2-10a), and (2-10b), yielding

$$\begin{bmatrix} A_2 \\ B_2 \end{bmatrix} = \chi_2 \begin{bmatrix} A_1 \\ B_1 \end{bmatrix} \tag{2-13a}$$

$$\begin{bmatrix} A_{1-} \\ B_{1-} \end{bmatrix} = 0 \tag{2-13b}$$

$$\begin{bmatrix} A_{1+} \\ B_{1+} \end{bmatrix} = \begin{bmatrix} A_{1-} \\ B_{1-} \end{bmatrix} + \frac{1}{\alpha_j}\begin{bmatrix} -K_0(\sigma_1 x') \\ I_0(\sigma_1 x') \end{bmatrix} \tag{2-13c}$$

$$\begin{bmatrix} A_2 \\ B_2 \end{bmatrix} = \chi_1 \begin{bmatrix} A_{1+} \\ B_{1+} \end{bmatrix} \tag{2-13d}$$

$$A_3 I_0(\sigma_3 R_3) + B_3 K_0(\sigma_3 R_3) = 0 \tag{2-13e}$$

where χ_i is a set of 2 by 2 matrixes given by

$$\chi_i(1,1) = \sigma_{i+1}X_i\{I_0(\sigma_i X_i)K_1(\sigma_{i+1}X_i) + \varepsilon_i I_1(\sigma_i X_i)[K_0(\sigma_{i+1}X_i) + \Omega_i K_1(\sigma_{i+1}X_i)]\},$$

$$\chi_i(1,2) = \sigma_{i+1}X_i\{K_0(\sigma_i X_i)K_1(\sigma_{i+1}X_i) - \varepsilon_i K_1(\sigma_i X_i)[K_0(\sigma_{i+1}X_i) + \Omega_i K_1(\sigma_{i+1}X_i)]\},$$

$$\chi_i(2,1) = \sigma_{i+1}X_i\{I_0(\sigma_i X_i)I_1(\sigma_{i+1}X_i) - \varepsilon_i I_1(\sigma_i X_i)[I_0(\sigma_{i+1}X_i) - \Omega_i I_1(\sigma_{i+1}X_i)]\},$$

$$\chi_i(2,2) = \sigma_{i+1}X_i\{K_0(\sigma_i X_i)I_1(\sigma_{i+1}X_i) + \varepsilon_i K_1(\sigma_i X_i)[I_0(\sigma_{i+1}X_i) - \Omega_i I_1(\sigma_{i+1}X_i)]\},$$

with $\varepsilon_i = \frac{k_i\sigma_i}{k_{i+1}\sigma_{i+1}} = \frac{k_i\sqrt{\alpha_{i+1}}}{k_{i+1}\sqrt{\alpha_i}}$ the ratio of effusivities of two neighboring layers and $\Omega_i = k_{i+1}\sigma_{i+1}X_{ci}$. The Wronskian identity has been applied in the reduction. The coefficients are eliminated from the equations, except those from the first and last layers, yielding

$$B_1 = 0 \tag{2-14}$$

$$\begin{bmatrix} A_3 \\ B_3 \end{bmatrix} = \gamma_3 \begin{bmatrix} A_1 \\ B_1 \end{bmatrix} + \frac{\gamma_2}{\alpha_1} \begin{bmatrix} -K_0(\sigma_1 x') \\ I_0(\sigma_1 x') \end{bmatrix} \tag{2-15}$$

$$A_3 I_0(\sigma_3 X_3) + B_3 K_0(\sigma_3 X_3) = 0 \tag{2-16}$$

where $\gamma_1 = \chi_1$, $\gamma_2 = \chi_2\chi_1$, and $\gamma_3 = \gamma_2\gamma_1$. A_1 is then determined from Eqs. (2-17),

$$A_1 = \frac{1}{\alpha_j} \frac{[\gamma_2(1,1) - \gamma_2(2,1)S]K_0(\sigma_j x') + [\gamma_2(2,2)S - \gamma_2(1,2)]I_0(\sigma_j x')}{\gamma_3(1,1) - \gamma_3(2,1)S} \tag{2-17}$$

with $S \equiv -K_0(\sigma_3 X_3)/I_0(\sigma_3 X_3)$. If $S \equiv K_1(\sigma_3 X_3)/I_1(\sigma_3 X_3)$, the solution is adapted for Neumann boundary condition at the outer surface $x = X_3$. Or, $S \equiv \frac{\sigma_3 k_3 K_1(\sigma_3 X_3) - hK_0(\sigma_3 X_3)}{\sigma_3 k_3 I_1(\sigma_3 X_3) + hI_0(\sigma_3 X_3)}$ for the third kind of BC.

The solution of the Green function is obtained by substituting all coefficients into Eqs. (2-11a) and (2-11b).

As heat generation may occur in any layer, temperature field at the probe point x is given by integrating the GF function over the entire domain, yielding

$$\tilde{T}_i(x,\omega) = \sum_{j=1}^{N} \frac{\alpha_j}{k_j} \int_{X_{j-1}}^{X_j} \tilde{g}(x',\omega) G_i(x|x';\omega) dx' \tag{2-18}$$

Its amplitude is given by $\left|\tilde{T}_i\,(x,\omega)\right|$, and phase by $\tan^{-1}[\mathrm{Im}(\tilde{T}_i)/\mathrm{Re}(\tilde{T}_i)]$.

Using the phase lag between fuel layer and heat sink from the Eq. 18) and thermal properties of each materials, the experiment result can be predicted through the simulation program, and inversely, curve fitting can be conducted on ordinary material to test the applicability of this measurement method for determining thermal diffusivity and conductivity.

In addition, the theoretical model can be first used to design experimental parameters for higher sensitivity and lower measurement uncertainty. For instance, the thickness of each layer should be selected for the design of experiment based on the sensitivity analysis in Section 3.2. And the type of materials for each layer is based on the actual experiment request.

3.0 Experiment

3.1 Experiment Setup

3.1.1 Experiment Device

Traditionally, the temperature measurement of solid materials uses thermocouples, but in this experiment, in order to avoid the time delay, which is caused by contact measurement device, the IR video camera is applied to measure the surface temperature of each layer. The IR video camera can measure the temperature field of a cross-section of multiple layers at the same time, and it can also collect average temperature of the plane along thickness. Although the IR video camera can only collect the temperature on the surface of the material, in this experiment, the fuel layer is homogeneously heated, and the temperature of each plane along x direction should be homogeneous. The focus of the experiment is the phase difference between fuel layer and heat sink, so effect of air in this problem is negligible.

The fuel layer is homogeneously heated through current. Wave generator and transistor are applied as the frequency adjusting device and switch in the electrical circuit.

3.1.1.1 IR Video Camera

A QFI InfraScope™ MWIR Temperature Mapping Microscope is used to record temperature change of sample along time. The device is shown as Figure 3. Through this device, it is easy to achieve the temperature change data on the position at the surface of each layer. The frame capture speed of the camera is 53.42 Hz, and the pixel resolution is 36 microns. The size of

each pixel is approximately 24 microns. Through this device, both temperature mappings of graphite (as fuel) and tool steel O1 (as heat sink) can be recorded and compared at the same time, which avoids the phase delay from the different equipment of the circuit.

The ordinary temperature mapping picture example is shown in Figure 4. The resolution of temperature mapping is 500*500 pixels. From temperature mapping picture, the temperature change of each pixel along time can be collected.

By using 1x scope, all three layers can be captured at the same time, which avoids the time delay from different devices.

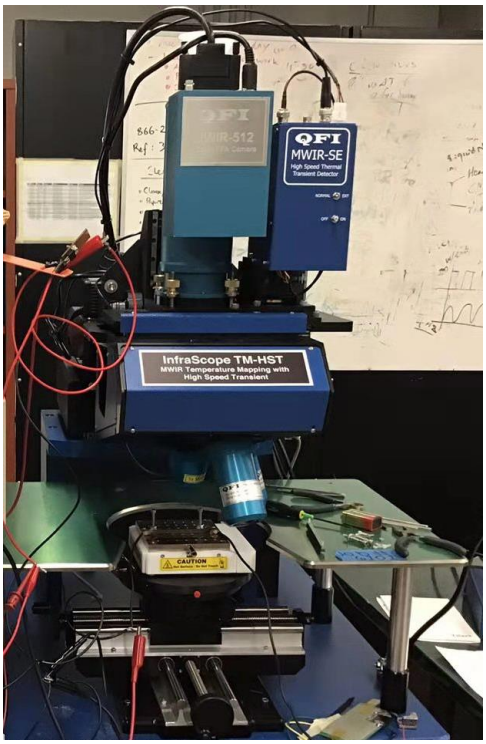

Figure 3. InfraScope™ MWIR Temperature Mapping Microscope

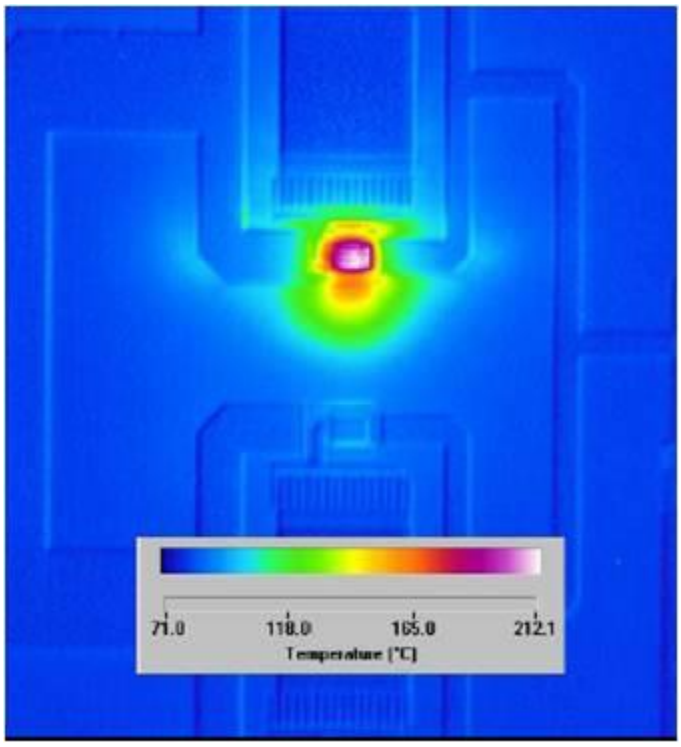

Figure 4. Temperature mapping

3.1.1.2 Heat Generation Circuit

In the experiment, in order to simulate the nuclear fuel and generate homogeneous heat flux in the fuel layer, constant current is applied in the circuit to control the heat generation rate. The circuit is showed in Figure 5. The electrical resistance of the graphite is 0.45 Ω. 8 A constant current is applied to generate heat in the sample, because the IR camera can only measure low temperature range, which is 15℃ to 200℃. The high temperature would increase the influence of thermal convection of the exposed surface of the sample. Normally, the temperature rise of fuel layer would be less than 40 degrees, with 8 A low frequency AC current. RFP70N06 transistor and Agilent wavefunction generator are applied to control the frequency of the heat flux.

A transistor is a semiconductor device used to amplify or switch electronic signals and electrical power. For RFP70N06 transistor, there are two paths inside it. One is the main path that

the current can pass through while the other is a switch gate that is used to control whether the main path is open or not. The main path will open when voltage larger than certain value is applied to the switch gate, and the electrical resistance of the main path will also decrease while the voltage grows. By using these characteristics of RFP70N06 transistor, it is easy to generate heat under certain frequency in the sample.

According to the comparison of different types of current wave, square wave is picked, in order to observe simpler and clearer temperature changing result of sample from the IR camera. The high-level voltage of square wave is 6 V, which can completely open the main pass of the transistor, and the low-level voltage of square wave is 0 V, which will completely close the transistor. The time of high-level voltage and low-level voltage is the same. The wave form of temperature change in the sample is close to the sawtooth wave. In the circuit, only fuel layer is directly connected to the power source, and heat sink is completely blocked from the current by the cladding layer.

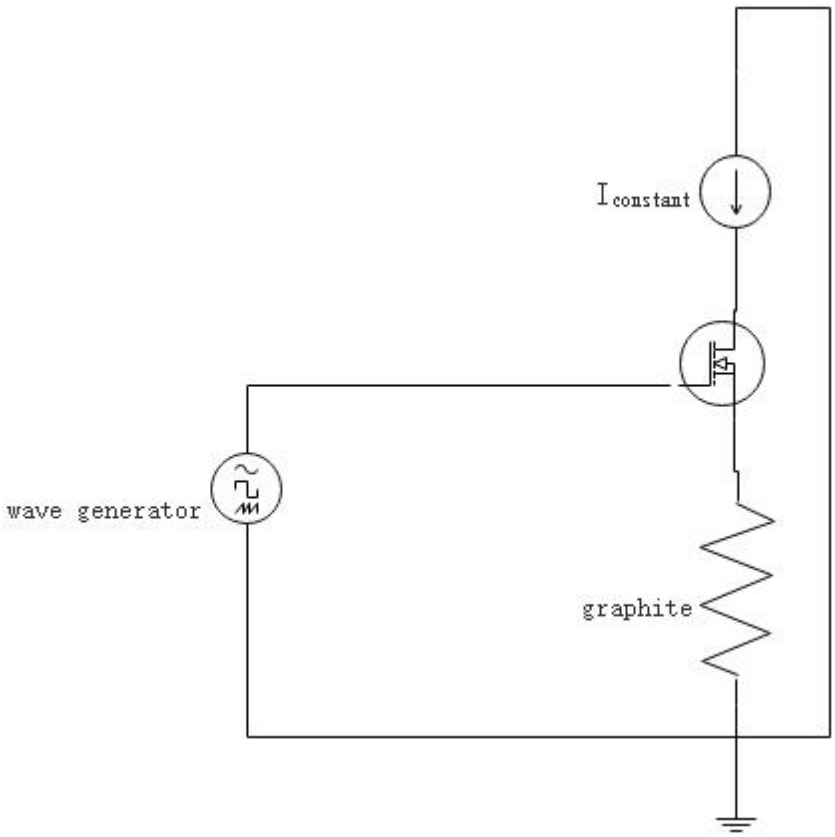

Figure 5. AC current heat generation circuit for the fuel layer

3.1.2 Sample Preparation

In this study, the assembly that mimics the test module in the transient reactor at the Idaho National Laboratory consists of a graphite bar which represents the fuel, and a tool steel O1 (TS O1) bar serving as heat sink. AC electric current is applied to generate a spatially uniform temperature oscillation (thermal wave) in the graphite bar. A thin layer of h-BN powder is sprayed between bars to provide electric isolation while allowing for good heat conduction. The model is shown as Figure 6. The length of the sample is 4 inches (101.6 mm), which is 10 times more than the thickness and width of the sample, so the length of the sample can be considered as infinite length. In addition, the width of the sample is 5 mm. Since the fuel layer is homogeneously heated

through current, and the temperature rise of each layer is less than 20 K, compared to the temperature of air, the heat transfer in the sample can still be considered as 1D heat transfer along thickness direction.

Thermal properties of each material are shown in the Table 1. The researcher used graphite as fuel layer because of its good thermal conductivity and high electric resistance, comparing to the metal materials. High thermal conductivity and high electric resistance, comparing to the metal, will allow low current to generate large temperature change. Due to the low accuracy of temperature measurement of the IR video camera, graphite is an ideal material for the experiment.

Using h-BN powder as cladding layer is because it can completely block the electricity from fuel layer to heat sink, and it also has good thermal conductivity.

Tool steel O1 was used due to its availability and ease of cutting to fit the size of the graphite.

In addition to these three materials, there is thermal contact resistance existing between graphite and h-BN powder layer, which is caused by mechanical contact between these two layers. Thermal contact resistance only exists between the fuel layer and the cladding layer because h-BN spray is used to generate cladding layer which completely covers the surface of heat sink. The fuel layer is connected to these two layers by screws.

Table 1. Properties of materials

Material type	Conductivity W/m*K	Diffusivity m^2/s	Density kg/m^3	Heat capacity J/kg*K
Graphite	83	64.2e-6	1820	710
h-BN	22.643	12.445e-6	2280	798
Tool Steel O1	64	17.78	7810	461

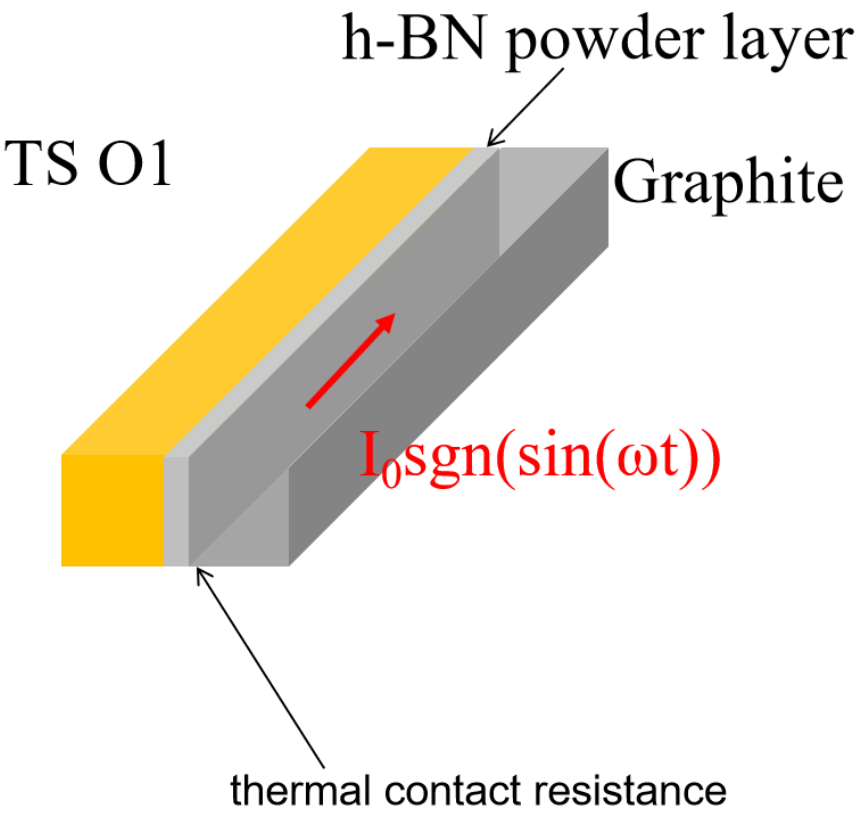

Figure 6. Sample model

3.2 Sensitivity Analysis

In order to determine the thickness of each layer, we use sensitivity analysis as reference to optimize the experiment design. Sensitivity is defined as

$$S(x) = \frac{\varphi[(\varepsilon + 1)x] - \varphi(x)}{\varepsilon}$$

where φ is the phase of the measure point, compared to the heat generation source. ε is a small rate of percentage change of parameter x.

High sensitivity means the perturbation of this parameter in the experiment has a very strong influence on the phase change result. And if target parameters have low sensitivity, there is a possibility that we cannot quantify it from the experiment result.

3.2.1 Determining of Thickness of Each Layer

Because the main purpose of this experiment is to test the technique of measuring thermal conductivity and diffusivity of the fuel layer, the influence of other properties of materials must be minimized in the design of experiment. In order to achieve this objective, the sensitivity analysis is used to determine the thickness of each layer.

Figure 7, Figure 8 & Figure 9 show the sensitivity distribution of thermal properties and thickness of each layer under different thickness of heat sink and heating frequency. The measuring point for temperature phase lag is in the middle of heat sink. X-axis is the frequency of the current, y-axis is the thickness of the heat sink, and the value of the line inside the figure shows the sensitivity of each property of different layers. In the sensitivity analysis, whether the value of sensitivity is positive, or negative is not important. What matters is the absolute value of the sensitivity. Because the sensitivity means the change of the result, which is caused by the variation of the parameters, for the parameters which need to be measured. For instance, the change of fuel property should cause temperature phase delay as large as possible for the experiment, which means the absolute value of sensitivity is as large as possible. The remaining parameters, their sensitivity or the effect on temperature phase delay change should be as small as possible.

In Figure 7, all three pictures show the sensitivity result of conductivity of each layer under different frequency and thickness of heat sink. The picture on the left above shows the sensitivity analysis result of conductivity of fuel layer. For the fuel layer, because the objective of the

experiment is to measure the conductivity and diffusivity of this layer, the range of selected thickness of heat sink and frequency should be located at the range where the sensitivity has the largest absolute value. Conversely, the other two pictures, which show the sensitivity analysis result of conductivity of the cladding layer and heat sink, show the selected range of thickness of heat sink and frequency. These diagrams show be the range where the absolute value of sensitivity is as small as possible.

In Figure 8, all three pictures show the sensitivity result of thermal diffusivity of each layer under different frequency and thickness of heat sink. The method of sensitivity analysis is the same as Figure 7. Thermal diffusivity of fuel layer has the largest absolute value of sensitivity and minimizes the sensitivity of the other two layers. In the left diagram below, the sensitivity of diffusivity of heat sink is close to the sensitivity of thermal diffusivity of fuel layer. For this reason, the value of thermal diffusivity of heat sink must be accurate.

In Figure 9, the diagrams show the sensitivity result of thickness of each layer under different frequency and thickness of the heat sink. Since the thickness of three layers isn't the measurement objective, the absolute value of sensitivity of thickness for each layer should be as small as possible. However, among all the range of thickness of heat sink and frequency that has been applied, the absolute value of sensitivity of the thickness of fuel layer and heat sink are always the largest ones among all parameters. For this reason, the experiment needs to have the high accuracy value of thickness of fuel layer and heat sink.

According the Figure 7, Figure 8 & Figure 9, the ideal frequency domain is [0.4, 0.7] Hz, and the ideal thickness domain of heat sink is [4, 10] mm.

The method of selecting the thickness of fuel layer and frequency from Figure 10, Figure 11, and Figure 12 is the same as selecting the thickness of heat sink.

According the Figure 10, Figure 11, and Figure 12, the ideal frequency domain is [0.4, 1.0] Hz, and the ideal thickness domain of fuel layer is [2, 4] mm.

In addition, the sensitivity of thickness of the cladding layer in this experiment is ignored because it has a very thin coating. The thickness of the cladding layer is in microns, and the thickness change in this level won't create much influence on the sensitivity of other parameters. What's more, due to the thin thickness of the cladding layer, the absolute value of sensitivity of all parameters of this layer is always very small.

The actual sample is show in Figure 13. In Figure 13, the black layer is graphite, which is the surrogate fuel layer, and the silver part is TS O1, which is heat sink. The cladding coating layer is too thin to see from the Figure 13. In addition, the screws that are used to connect samples are made of plastic. The electric current can only pass through nuts and graphite. The metal pieces on the two ends of the sample are copper plates, which are used to fix the wires.

The thickness of the fuel layer in the actual sample is 1/4 inch, which is equal to 3.175 mm. The thickness of the cladding layer in the actual sample is 0.145 mm. And the thickness of heat sink in the actual sample is 3/16 inch, which is equal to 4.7625 mm. The accuracy of the thickness of the fuel layer and heat sink is ± 0.0001 mm.

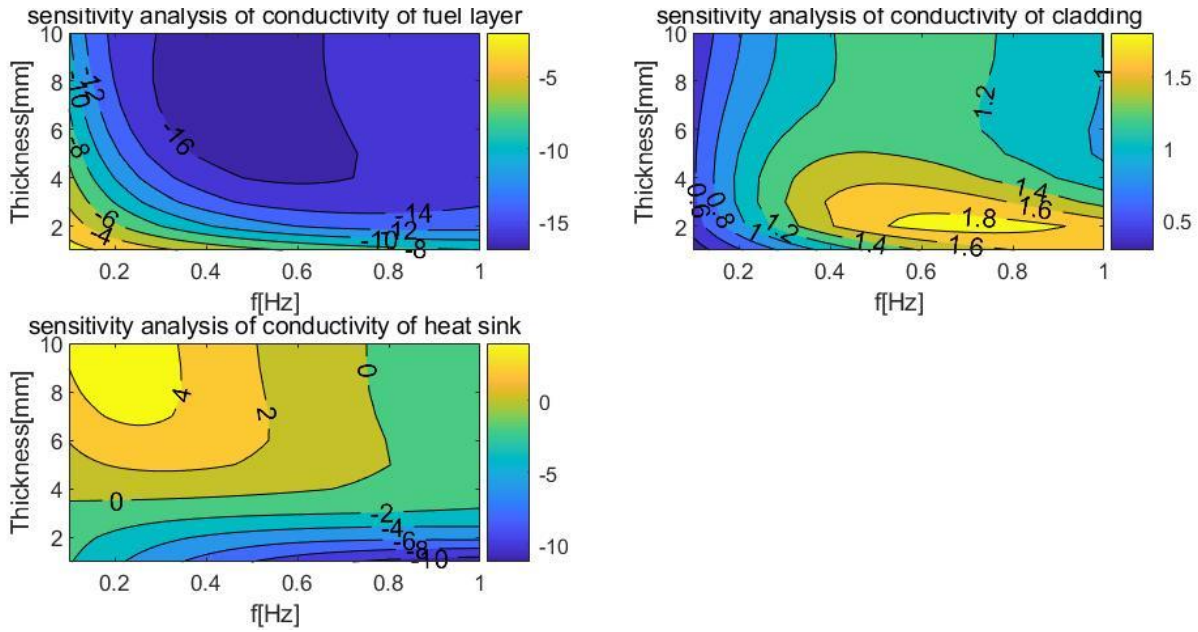

Figure 7. Sensitivity analysis of conductivity of each layer for selecting heat sink thickness and frequency

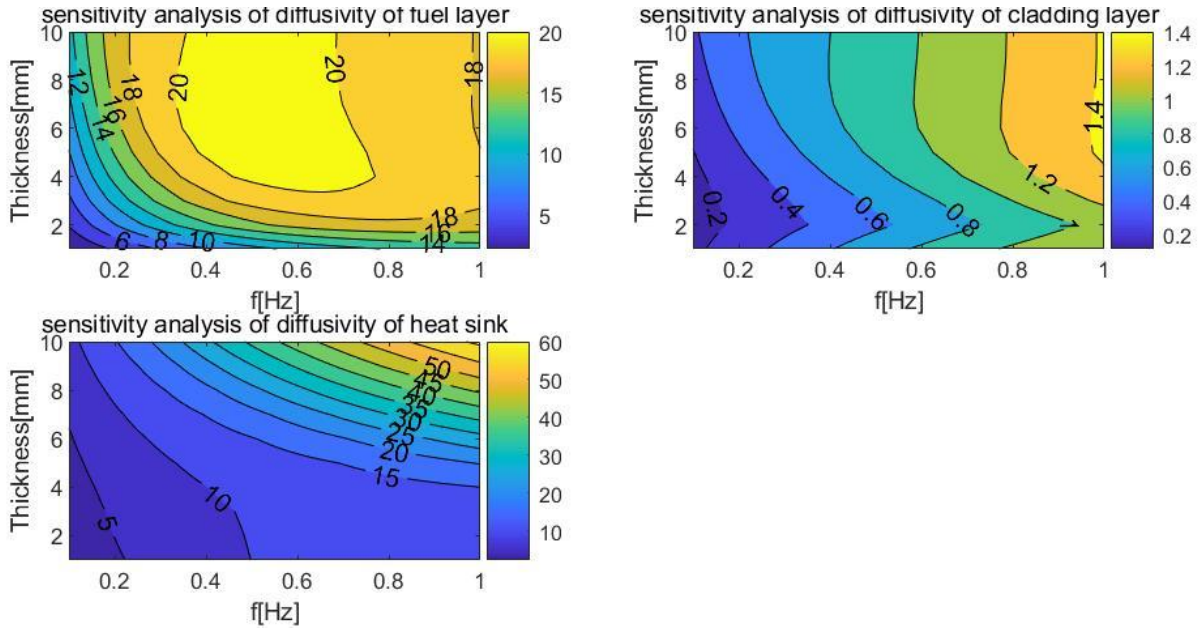

Figure 8. Sensitivity analysis of diffusivity of each layer for selecting heat sink thickness and frequency

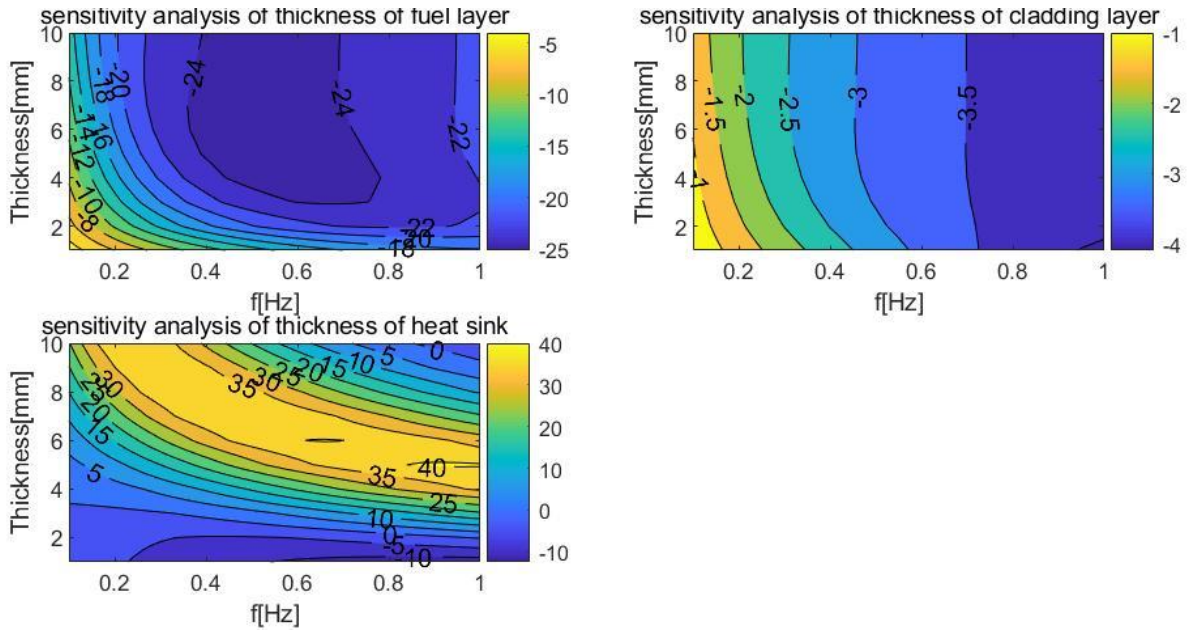

Figure 9. Sensitivity analysis of thickness of each layer for selecting heat sink thickness and frequency

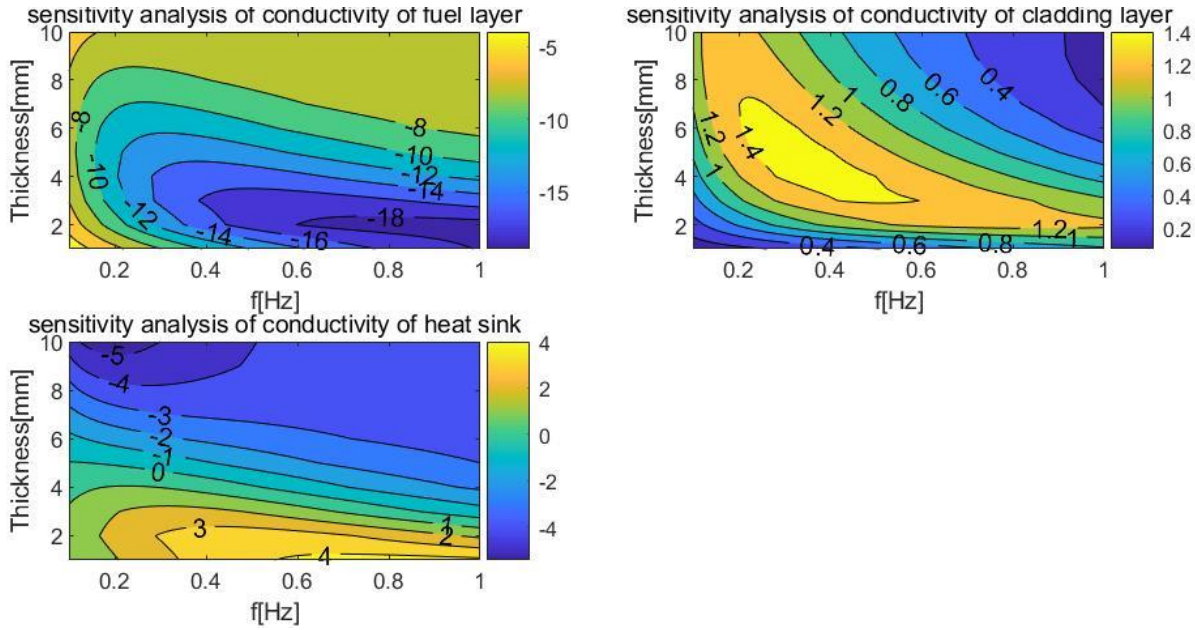

Figure 10. Sensitivity analysis of conductivity of each layer for selecting fuel layer thickness and frequency

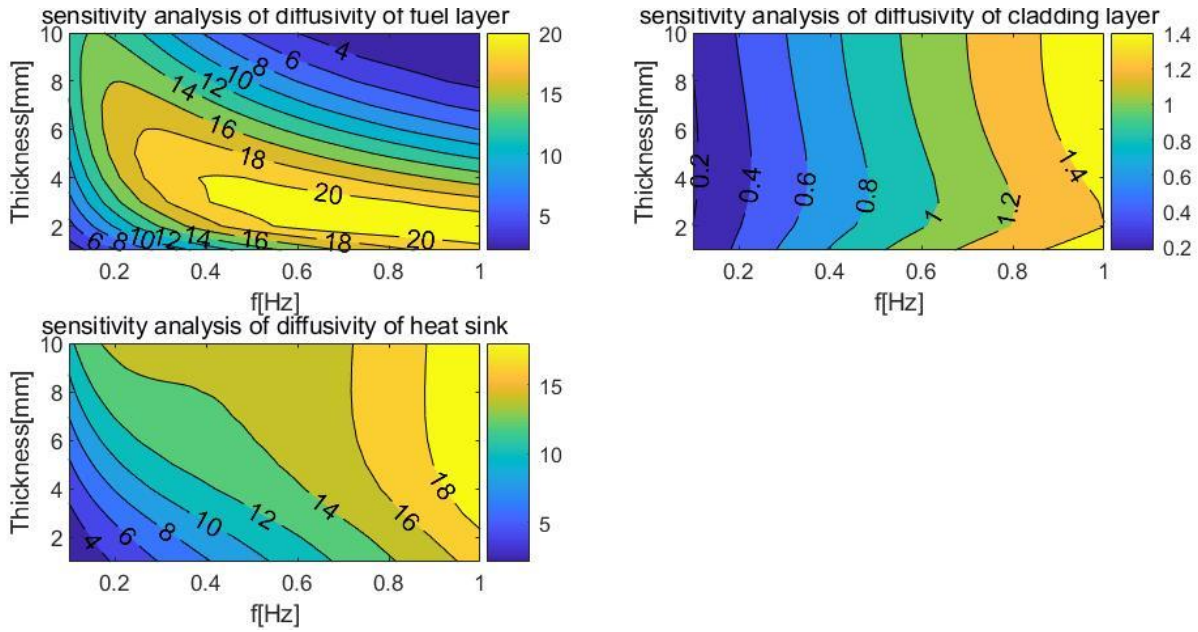

Figure 11. Sensitivity analysis of diffusivity of each layer for selecting fuel layer thickness and frequency

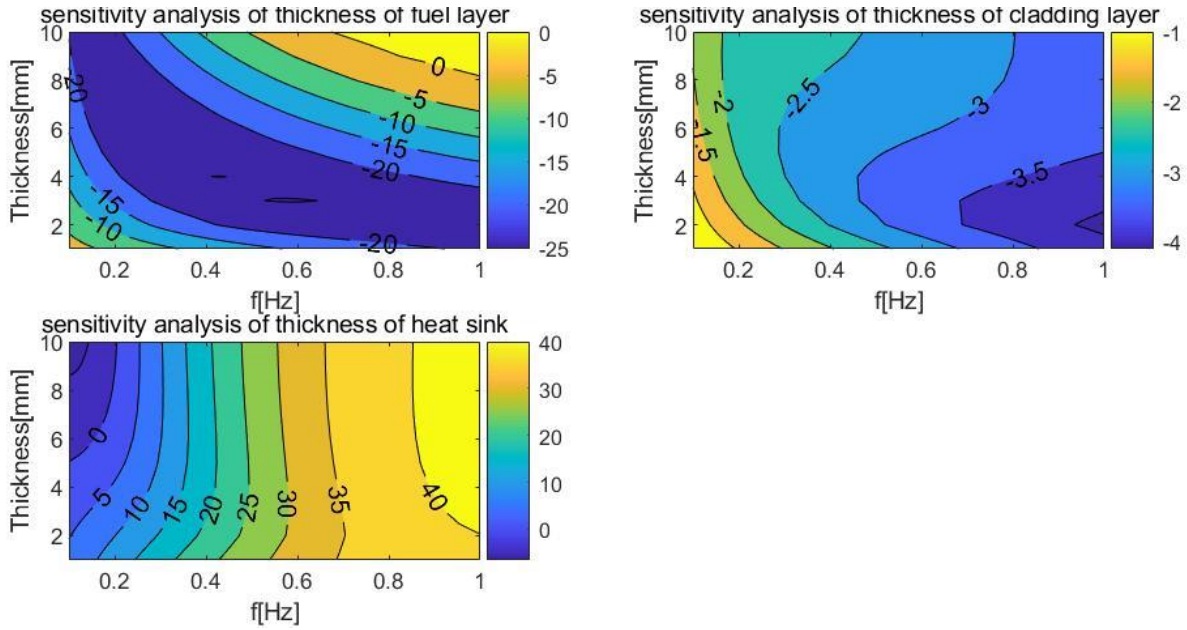

Figure 12. Sensitivity analysis of thickness of each layer for selecting fuel layer thickness and frequency

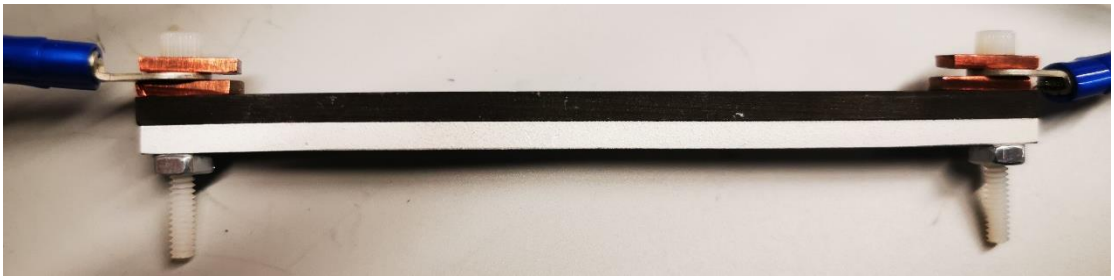

Figure 13. The actual sample

3.2.2 Impact of Thermal Diffusivity

After selecting the thickness of each layer, sensitivity analysis can also be used to analyze the impact of each parameter in a frequency range. In Figure 14 and Figure 15, alpha1 means the thermal diffusivity of the fuel layer, which is the first layer, and alpha2 and alpha3 are the diffusivity of the cladding layer and heat sink.

According to Figure 14, it is clear that α_1 has the strongest sensitivity among all three layers, and the sensitivity of α_2 can basically be ignored. The low sensitivity of α_2 is due to the thin cladding layer, which is less than 10% of the other two layers.

Figure 15 shows the sensitivity analysis result of diffusivity of each layer along distance, which is the distance between the measuring point on heat sink and the interface of the cladding layer and heat sink, under 0.5 Hz. In addition, sensitivity analysis of diffusivity under other frequencies has also been conducted that the sensitivity of α_1 and α_2, on the different measuring point under certain frequency, are always constant. And sensitivity of α_3 increases with x.

From these two figures, the selecting of the thickness of each layer works as it's expected. Thermal diffusivity of fuel layer has the strongest sensitivity, comparing to thermal diffusivity of other layers. In addition, the trend of sensitivity of thermal diffusivity of each layer are all different along space or frequency, which means the curve fitting can be conducted either along frequency

or along space, unless other parameters show the same trend as thermal diffusivity of fuel layer along frequency or space.

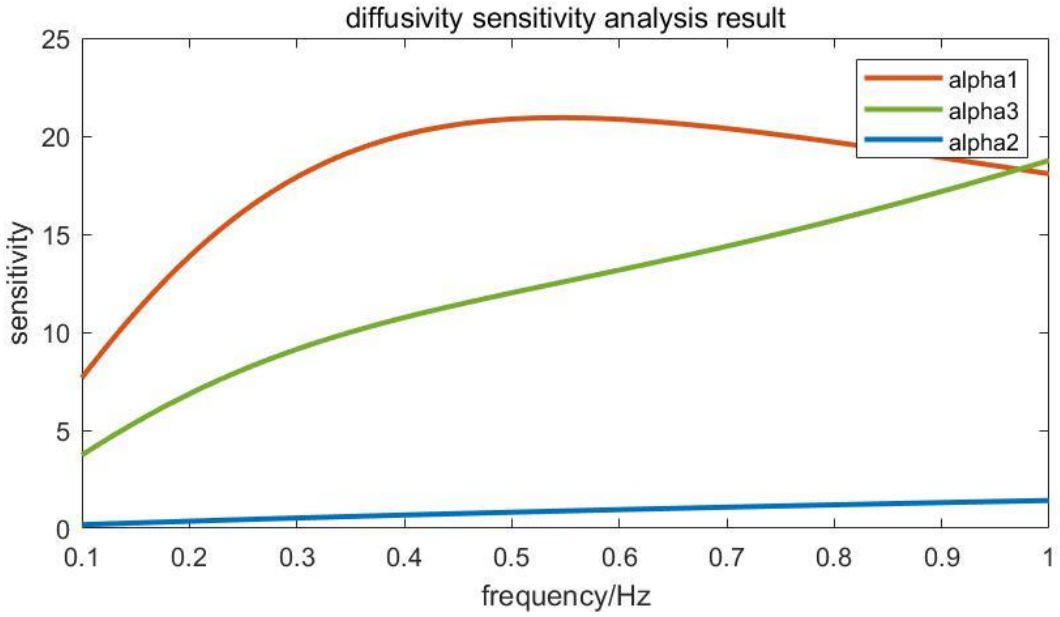

Figure 14. Sensitivity analysis of diffusivity along frequency

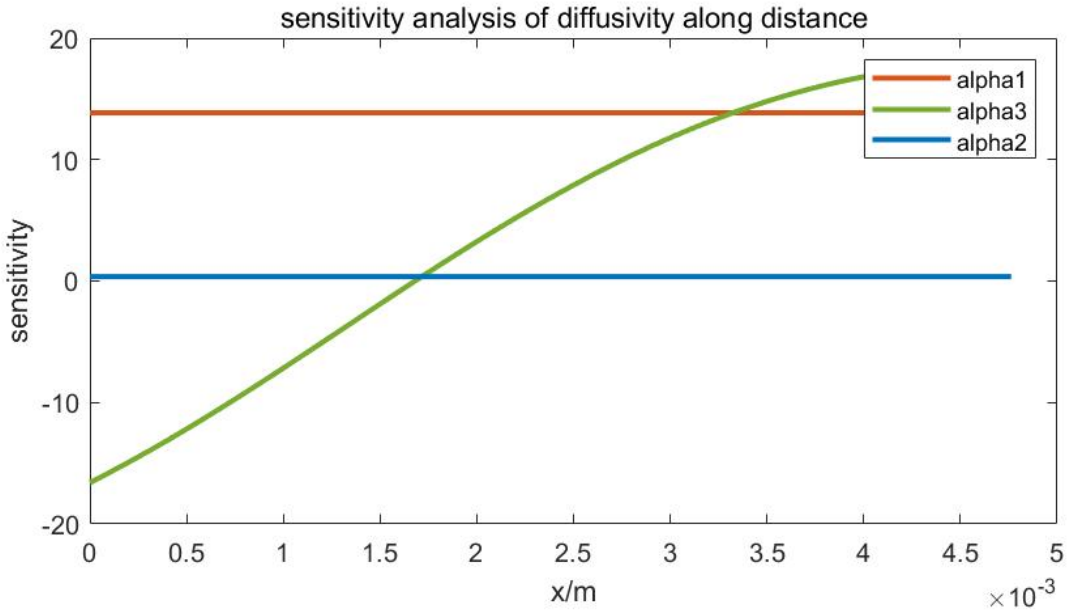

Figure 15. Sensitivity analysis of diffusivity along distance

3.2.3 Impact of Thermal Conductivity

Figure 16 shows the comparison of sensitivity of conductivity of each layer. The conductivity of fuel layer is designated as k1, the conductivity of cladding layer is k2, and the conductivity of heat sink is k3. The sensitivity of k_2 and k_3 are close to zero and k_1 has high sensitivity along frequency. Figure 17 shows the sensitivity analysis result of conductivity of each layer along distance under 0.5 Hz. All three sensitivity of conductivity is constant along frequency under certain frequency. From these two figures, due to the same trend of thermal conductivity and diffusivity of fuel layer, curve fitting cannot be conducted along space. The selecting of thickness of each layer works as it's expected.

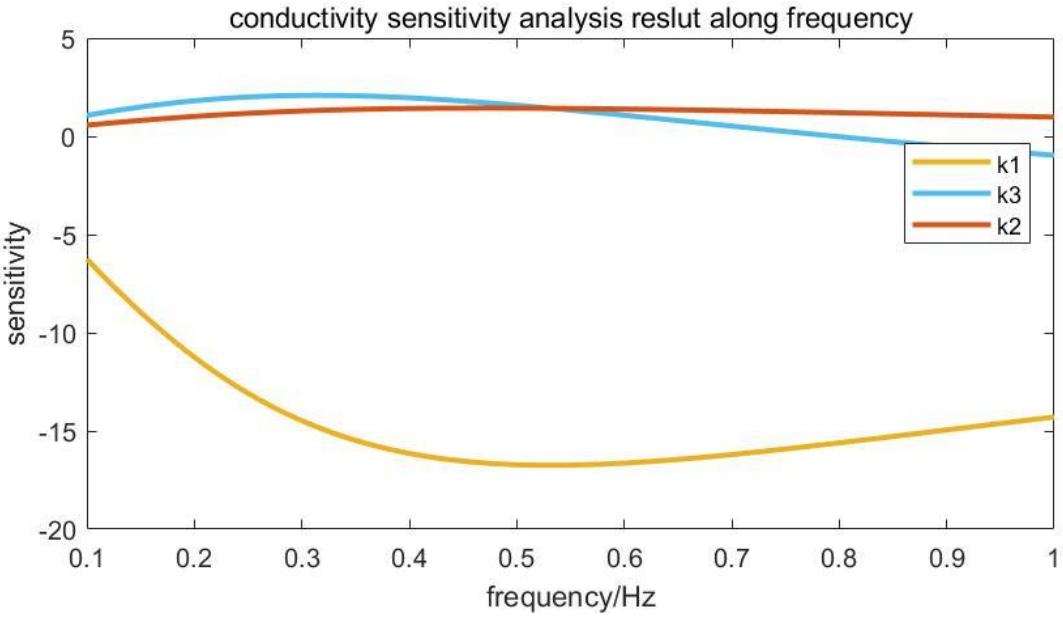

Figure 16. Sensitivity analysis of conductivity along frequency

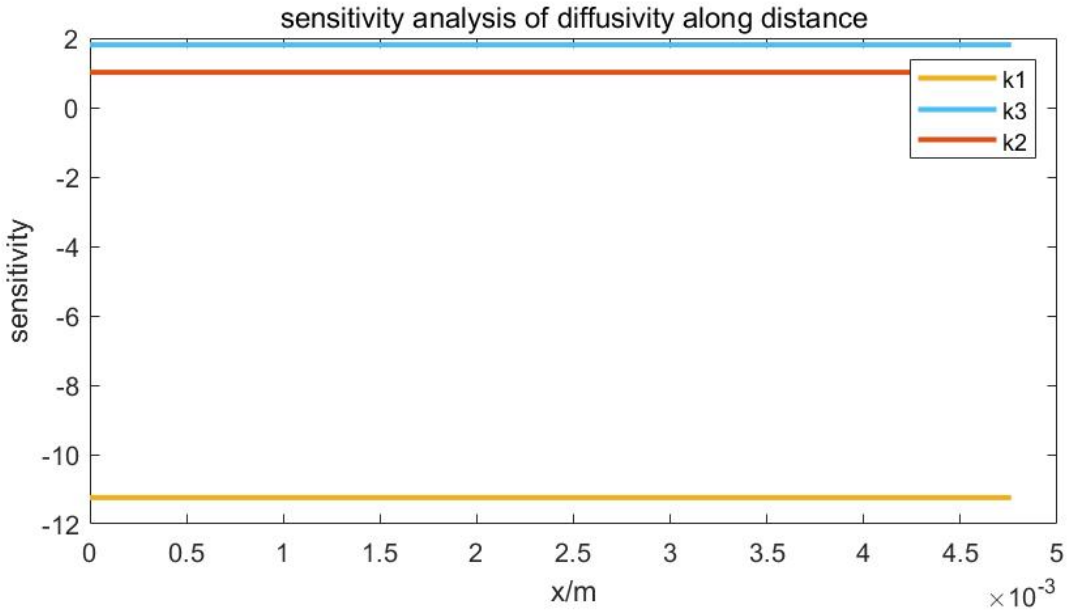

Figure 17. Sensitivity analysis of conductivity along distance

3.2.4 Impact of Thickness

Figure 18 shows the comparison of sensitivity of all parameters. Rth means the thermal contact resistance between the fuel layer and the cladding layer. The highlighted three lines are the sensitivity of thickness of each layer. L_1 is the thickness of fuel layer, L_2 and L_3 are the thicknesses of the cladding layer and the heat sink. Excluding L_2, the other two thicknesses have very high sensitivity along frequency axis which means if the accuracy of thickness of these two layers is low, the final measurement result of the thermal properties of the fuel layer would have a large error.

Figure 19 shows the sensitivity analysis result of thickness of each layer along distance under 0.5 Hz. In addition, sensitivity analysis of diffusivity under other frequency has also been conducted. The sensitivity of L_1 and L_2, on the different measuring point under certain frequency, are always constant and the sensitivity of L_3 decreases along x.

From these two figures, due to the high sensitivity of the thickness of fuel layer and heat sink, the accuracy of the thickness of these two layers must be high, in order to minimize the error caused by the thickness. In addition, although curve fitting cannot be conducted along space to measure thermal diffusivity of fuel layer, it can be used to check thermal diffusivity and thickness of heat sink in the experiment.

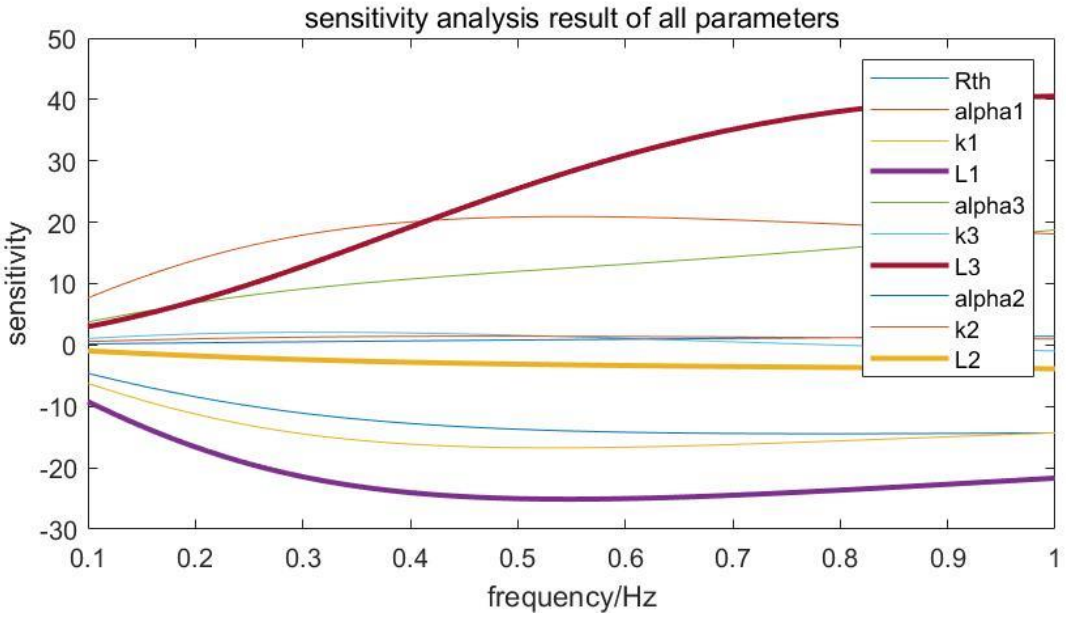

Figure 18. Sensitivity analysis of thickness along frequency

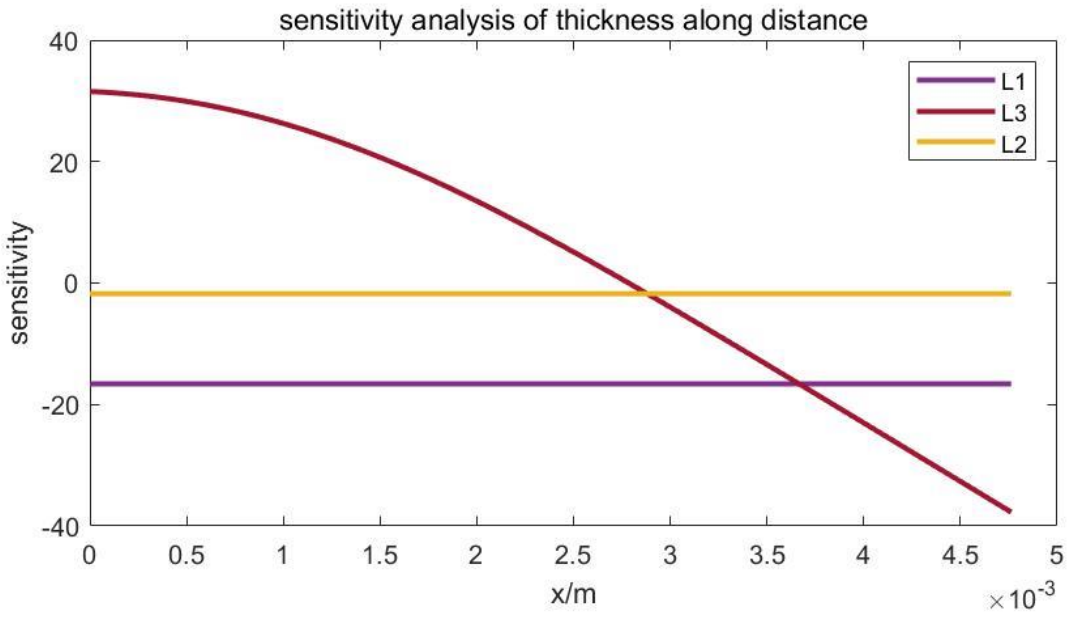

Figure 19. Sensitivity analysis of thickness along distance

3.2.5 Impact of Thermal Contact Resistance

After eliminating the uncertainty of the thickness of each layer, the sensitivity of thermal contact resistance is substantial among the other parameters. The sensitivity of thermal contact resistance is shown as Rth in Figure 20. The thermal contact resistance is a result of the poor contacts between the fuel layer and the cladding layer. The cladding layer is h-BN powder coating on the heat sink, which is perfectly bonded with each other. The fuel layer and the cladding layer are connected through compression by bolts on the ends of the sample. Due to the imperfect connection of these two surfaces, microscopic gaps, caused by surface roughness exists between these two layers. The influence can be equivalently described by a thermal contact resistance in the simulation program. Nevertheless, the actual value of thermal contact resistance is unknown. In this experiment, there is no device or technique to obtain the accurate value of thermal contact

resistance and eliminate the influence of this parameter. For these reasons, thermal contact resistance must be considered as one of the unknown parameters, like thermal diffusivity and conductivity of fuel layer, and be fitted together from the experimental data in a similar way to the actual reactor experiment.

Figure 20 and Figure 21 show the sensitivity analysis result of all parameters along frequency and x. Thermal contact resistance of these two figures is fitted from the same experiment. The highlighted blue line shows the change of sensitivity of thermal contact resistance (Rth) along frequency and x. As shown in Figure 20, sensitivity of Rth is one of the largest values among all parameters, except the thickness of each layer. The trend of Rth, α_1, and k_1 are different along frequency, which means that the curve fitting along frequency is possible to acquire the thermal properties of fuel layer and thermal contact resistance. However, in Figure 21, the sensitivity of Rth is a constant value, like the sensitivity of the most other parameters. For this reason, unless the accurate value of thermal contact resistance can be determined, curve fitting cannot be applied along x, but this condition can still be used to check the current value of thermal contact resistance of curve fitting along frequency.

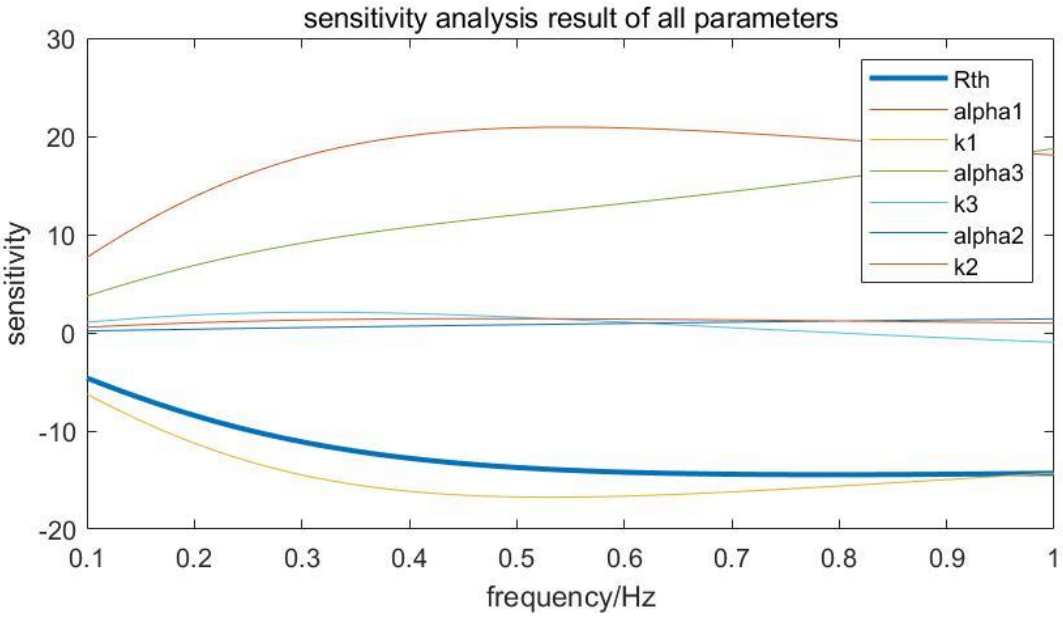

Figure 20. Sensitivity analysis of all parameters along frequency

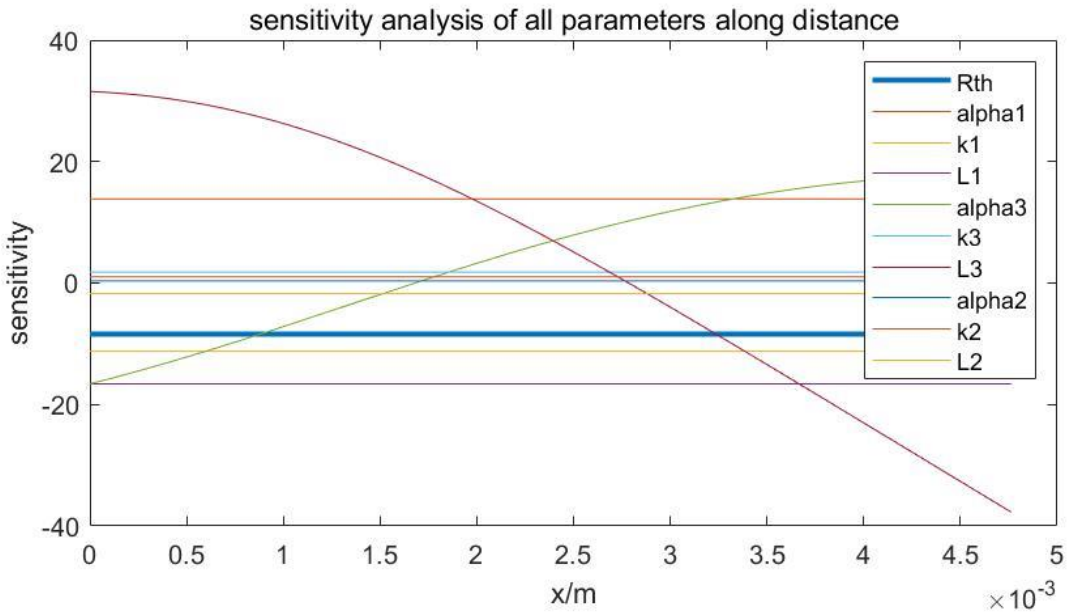

Figure 21. Sensitivity analysis result of all parameters along distance between measuring point on heat sink and connecting surface of the cladding layer and heat sink

3.2.6 Conclusion for Sensitivity Analysis

According to the sensitivity analysis above, in order to test the applicability of the method of measuring thermal diffusivity of fuel layer, the data must be collected under different frequencies. Based on the existence of thermal contact resistance, the phase data along distance on heat sink is useless for measuring thermal diffusivity of fuel layer. In addition, in order to improve the accuracy of measurement of thermal diffusivity of fuel layer, the thickness of each layer must be accurate.

3.3 Data Processing

Figure 22 shows the temperature mapping picture of sample and temperature change along time of fuel layer and heat sink. In Figure 22, the frequency of temperature is 0.5 Hz. After temperature data is collected, Fast Fourier Transfer (FFT) analysis method is applied to process the data and calculate the phase difference between the temperature change of fuel layer and heat sink. For example, in Figure 23 & Figure 24, Figure 23 shows when f = 0.5058 Hz, the temperature change wave has the highest amplitude. This means the frequency of temperature change is almost 0.5 Hz. The error of frequency is mainly caused by the data collecting speed of the IR camera, which is 53.42 Hz. X is the distance between the measuring point and the connecting surface of the cladding layer and heat sink.

According to the analysis result of Figure 23, the phase of temperature change wave function can be determined from Figure 24, which shows the phase of temperature change wave function along all frequency. The single value of phase of either fuel layer or heat sink is useless. During the experiment, the temperature data is always collected while the temperature of sample is under steady state. In addition, the phase of fuel layer should be homogeneous because it is homogeneously heated, and the experiment result has also proven that the fuel layer is homogeneously heated. The temperature change on the fuel layer is show in Figure 25. X is the distance between the end of the fuel layer and the connecting surface of the cladding layer and fuel layer. For the research, the valuable phase data is the difference of phase between measuring point on heat sink and fuel layer. Theoretically, the phase difference should be less than 0° and should decrease along the measuring point moving from the connecting surface between the cladding layer and heat sink to the other end of heat sink.

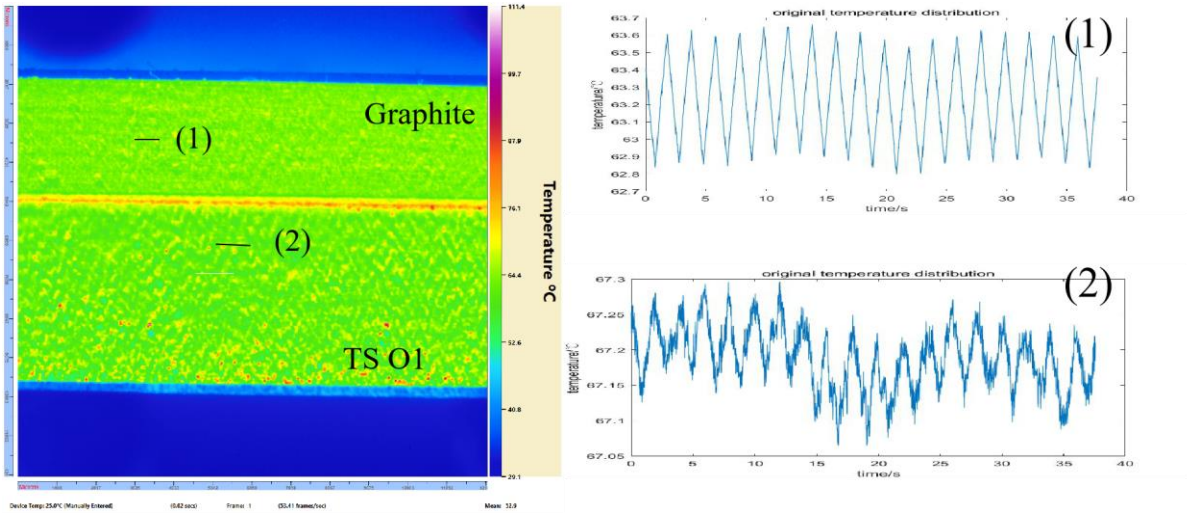

Figure 22. Temperature mapping and data collecting

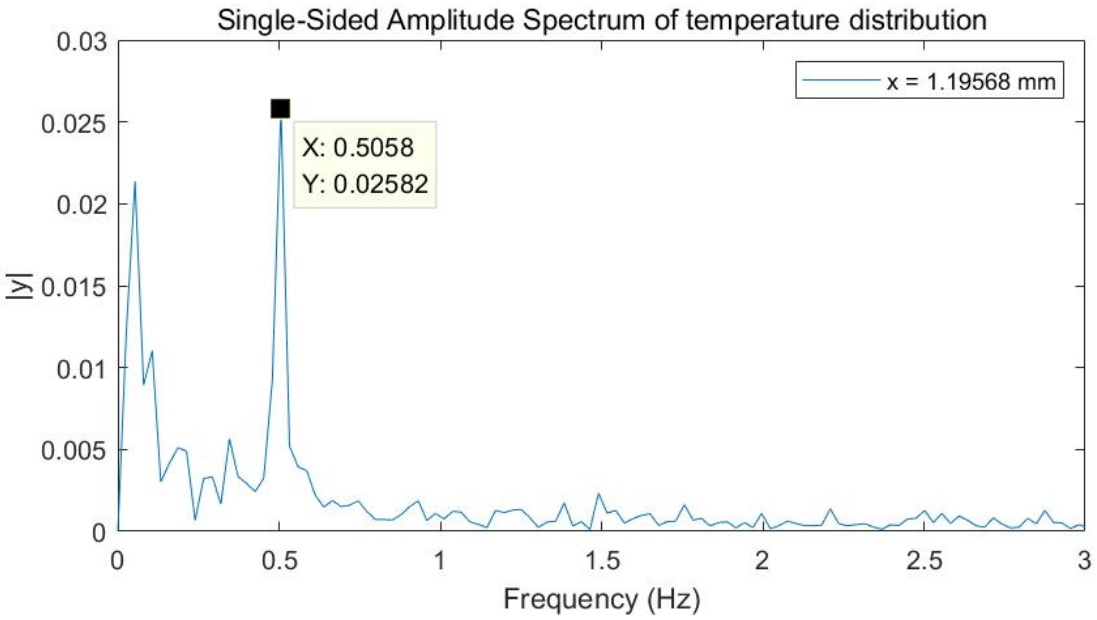

Figure 23. FFT analysis result of temperature amplitude

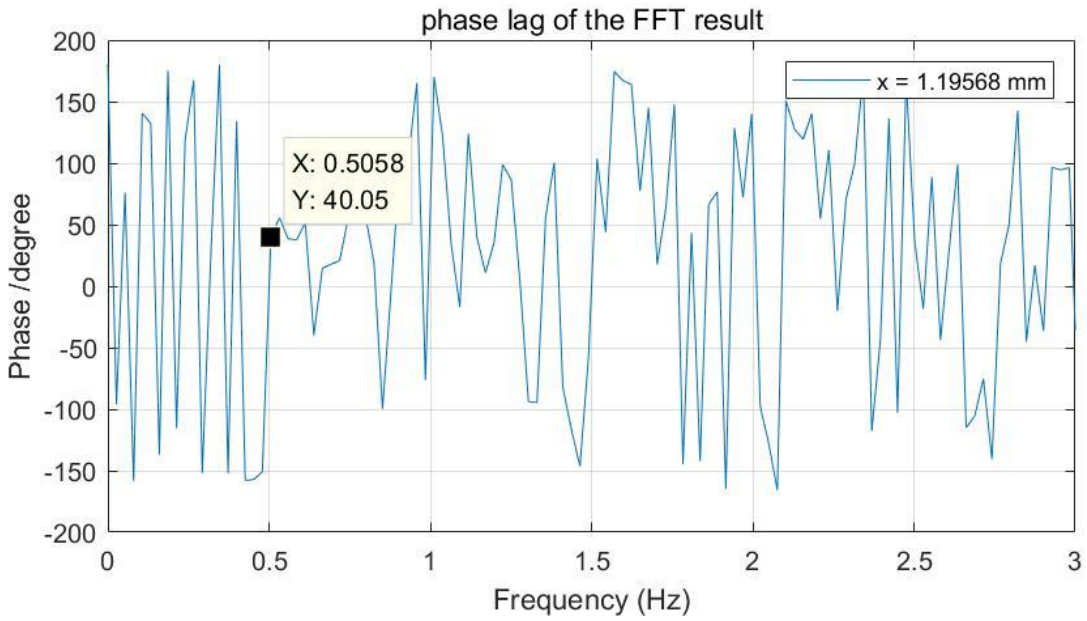

Figure 24. FFT analysis result of phase

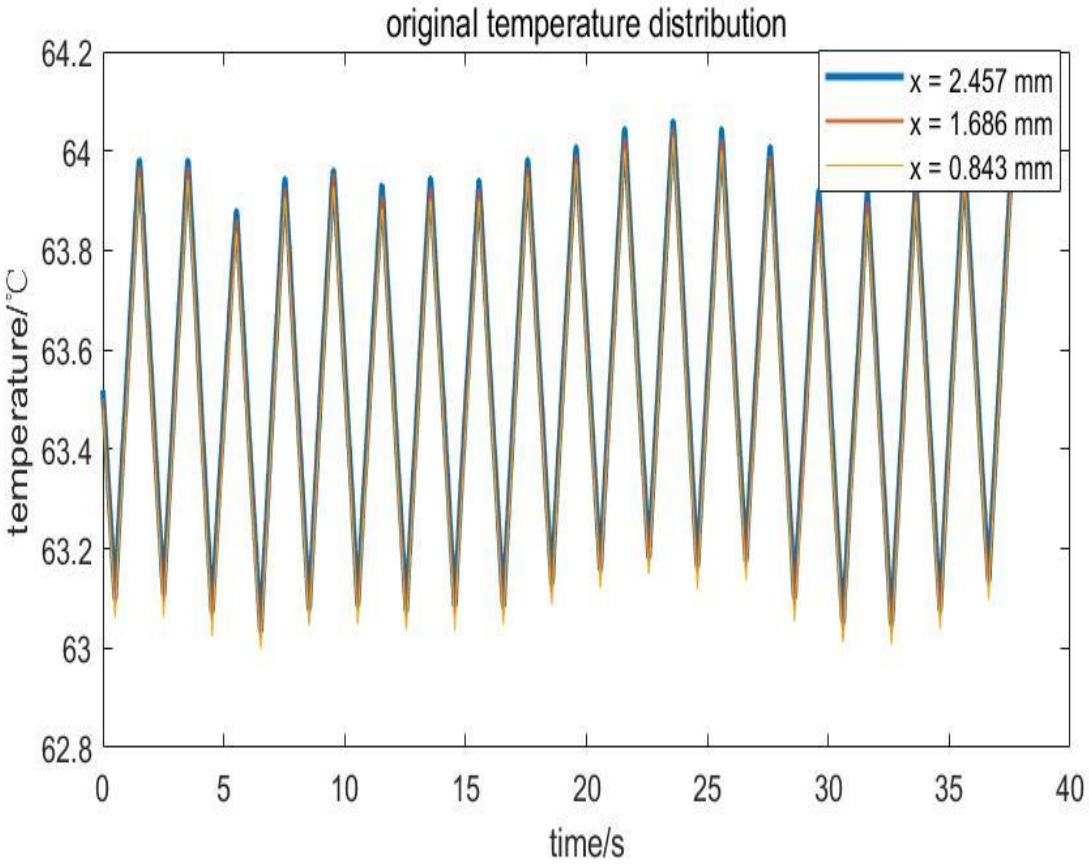

Figure 25. Temperature of different measuring point on the fuel layer

4.0 Result and Discussion

4.1 Existence of Thermal Contact Resistance

Because the thermal contact resistance was initially not designed to be directly measured, in order to prove the existence of it and determine its value, phase lag data along x direction must be collected. The original point of x is the connected surface between heat sink and cladding layer, and the direction of x is shown as Figure 26.

As shown in Figure 27, the blue line is the program simulation result, and the orange line is the data collected from the experiment. Figure 27 is the first version of comparison between experimental result and simulation result. At first, the experiment model didn't consider the existence of thermal contact resistance, so these two results show great difference between each other. From Figure 27, it's obvious that while not considering the existence of thermal contact resistance, the experimental result has shown a huge difference, compared to the simulation result.

In Figure 28, the influence of thermal contact resistance is considered and the accurate value of it is fitted through the program. The comparison with the same group of experiment data is shown in the figure. It's clear that experimental result fit the theoretical prediction. The same comparison has also been done under other frequencies, and the experimental data can always fit theoretical prediction well.

This is a method to measure thermal contact resistance between the cladding layer and fuel layer. The reason that thermal contact resistance is not observable between the cladding layer and heat sink is that while preparing the sample, the cladding layer is made with h-BN powder spray

on the surface of heat sink. The cladding layer is directly generated on the surface of heat sink. For this reason, the thermal contact resistance only exists between the cladding layer and the fuel layer.

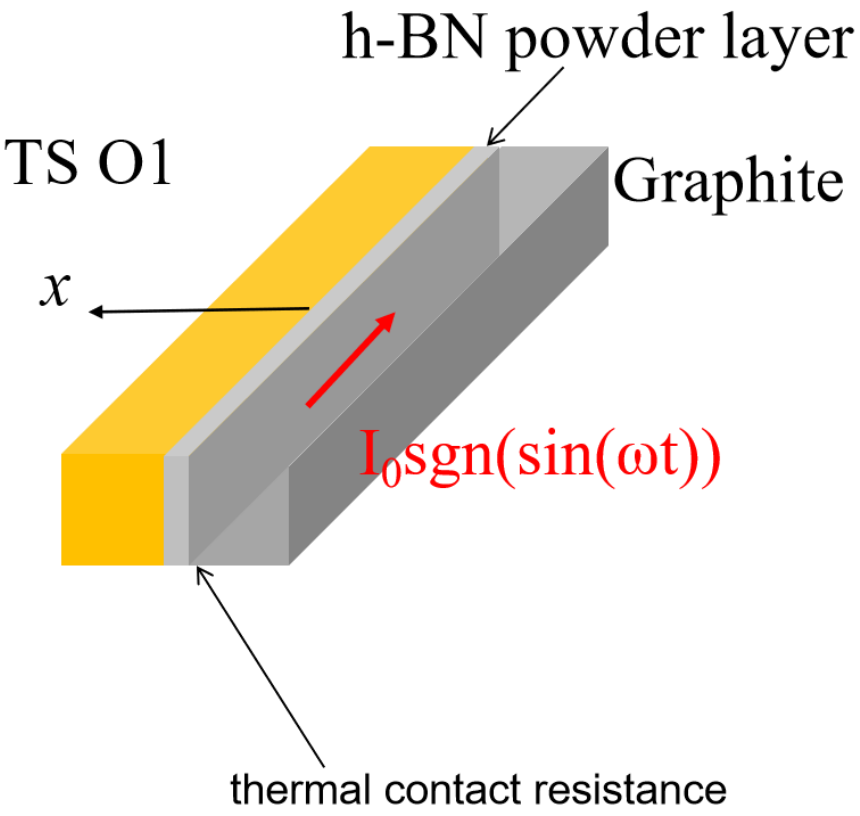

Figure 26. Sample model

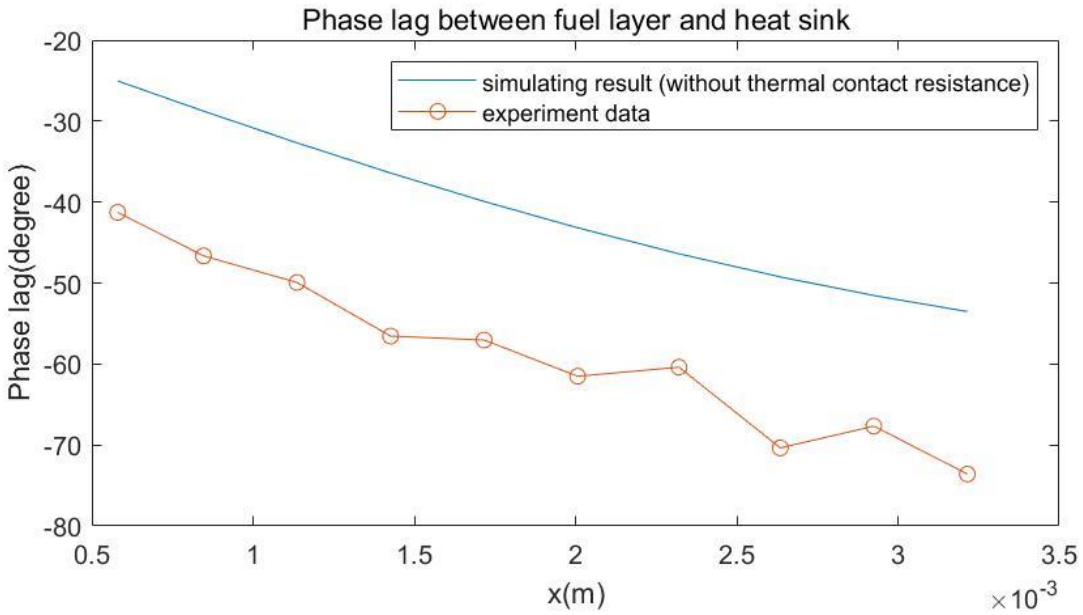

Figure 27. Phase lag comparison between experiment result and simulation result while not considering the influence of thermal contact resistance

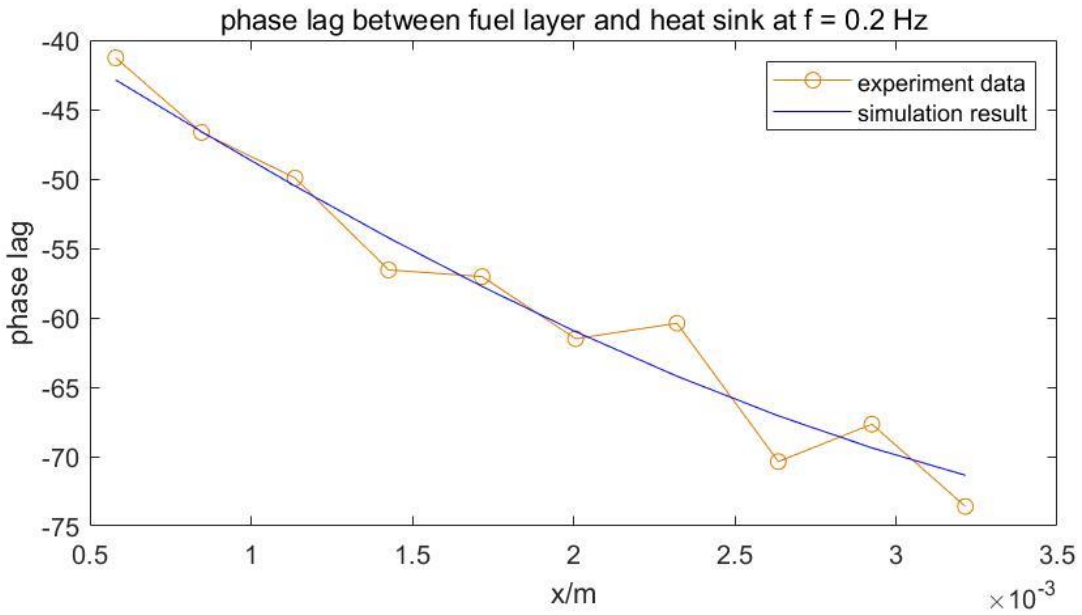

Figure 28. Phase lag comparison between experiment result and simulation result while considering the influence of thermal contact resistance (current value of thermal contact resistance is equal to 4.8166e-5 K/W)

4.2 Change of Thermal Contact Resistance

In the experiment, curve fitting is conducted for the data that is collected under the same frequency and different measuring point. Through this method, the actual value of thermal contact resistance can be determined. In addition, the experiment under different frequency means that for each frequency, the data is collected from the same sample while it is at steady state.

However, during the experiment, thermal contact resistance between the fuel layer and the cladding layer is found to be not a constant value. This change of resistance at different heating frequencies greatly complicates the method measuring thermal diffusivity of fuel layer in 1D plate. As an example, in one experiment, phase lag between fuel layer and heat sink is collected under different frequency. The result is shown as Figure 29. The blue line is the simulating result and the

purple line is the experiment data. The trend of these two lines is completely opposite. Fortunately, the phase lag along the x direction has also been collected from the same group of data because the IR video images contain temperature distribution along thickness direction. At this point, the experiment data and simulating result can fit well with each other, but the thermal contact resistance under each frequency is found to be different.

The first attempt was to find out the reason for change of thermal contact resistance and try to minimize its value. A lot of groups of data are collected under different frequency to characterize the thermal resistance.

Figure 30, Figure 31, Figure 32 and Figure 33 show, under different frequency, the actual value of thermal contact resistance of this experiment would have a large variation. Among these 4 groups of data, the largest value of thermal contact resistance is almost 10 times larger than the smallest value of it. Due to the large change of thermal contact resistance under different frequencies, it is impossible to conduct curve fitting to measure the thermal diffusivity of fuel layer using a fixed thermal resistance value.

After repeating the same experiment several times, at this time, there is no clear relationship between frequency and thermal contact resistance has been found. But considering the thermal contact resistance is caused by mechanical contact between the fuel layer and the cladding layer, the change of thermal contact resistance must be caused by the change of the mechanical contact between these two layers because interface contact resistance in this case has to be a function of the compression force pressing the two surface together. If the mechanical compression of these two layers can be fixed, the change of thermal contact resistance will be minimized or even erased.

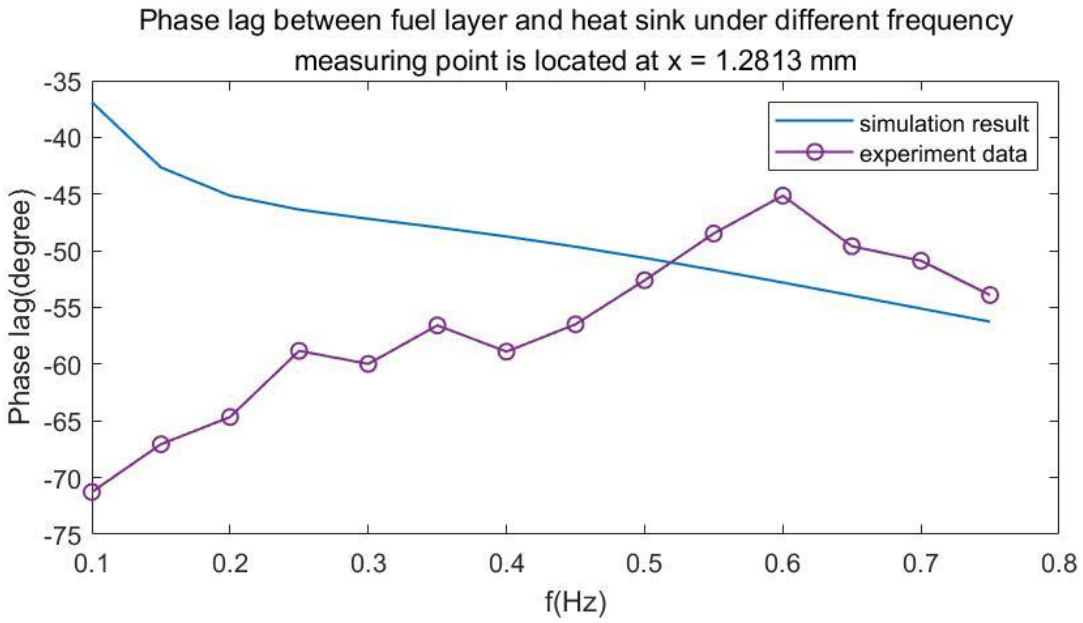

Figure 29. Comparison of phase lag between experiment data and simulation result under different frequency

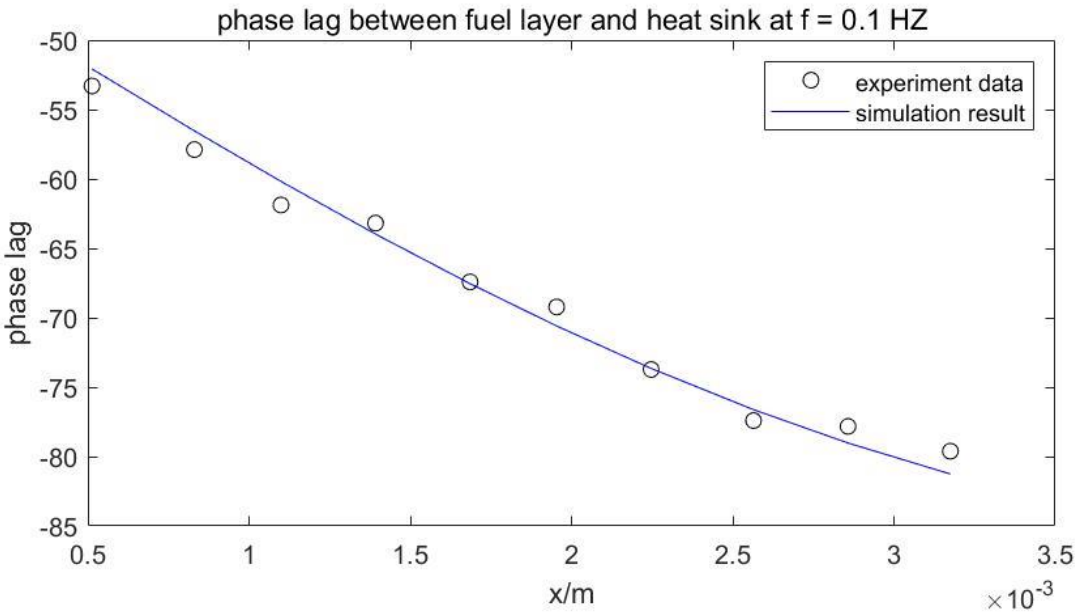

Figure 30. Phase lag comparison at f = 0.10 Hz (value of thermal contact resistance is equal to 2.1918e-04 K/W)

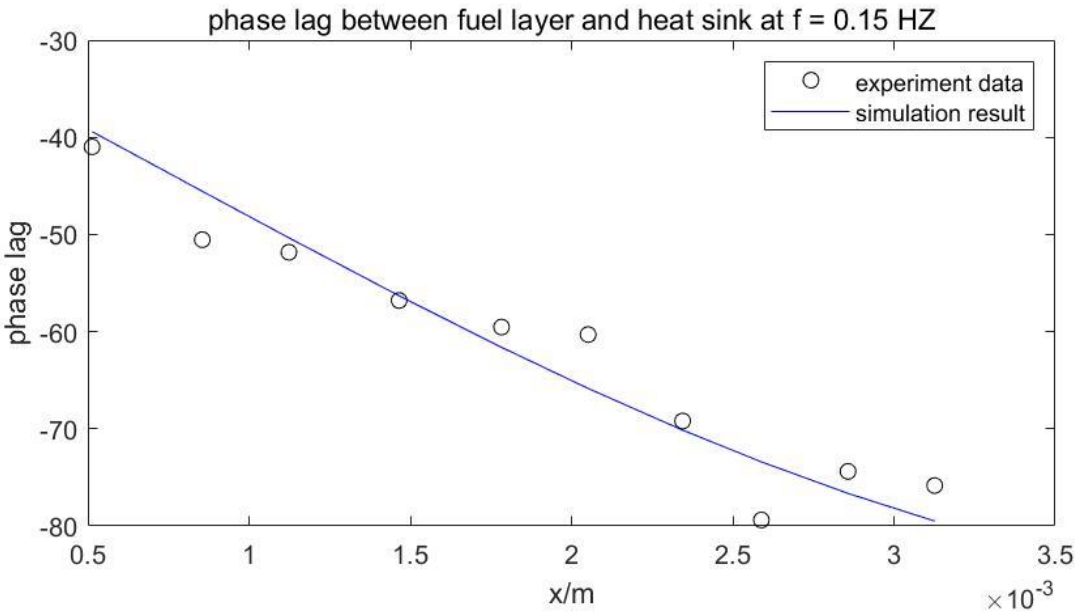

Figure 31. Phase lag comparison at f = 0.15 Hz (value of thermal contact resistance is equal to 8.3100e-05 K/W)

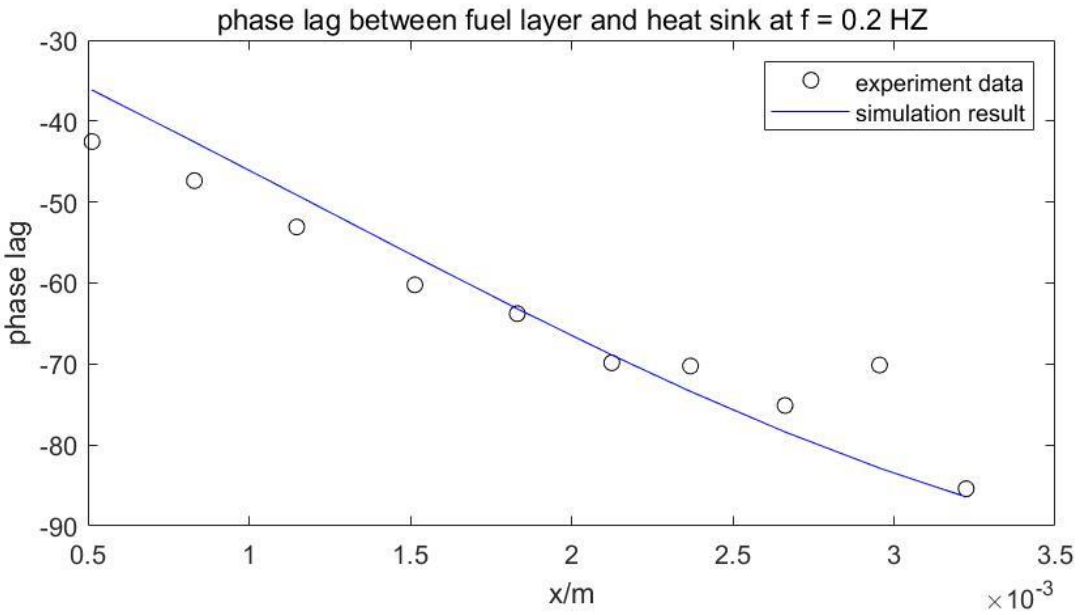

Figure 32. Phase lag comparison at f = 0.20 Hz (value of thermal contact resistance is equal to 6.3281e-05 K/W)

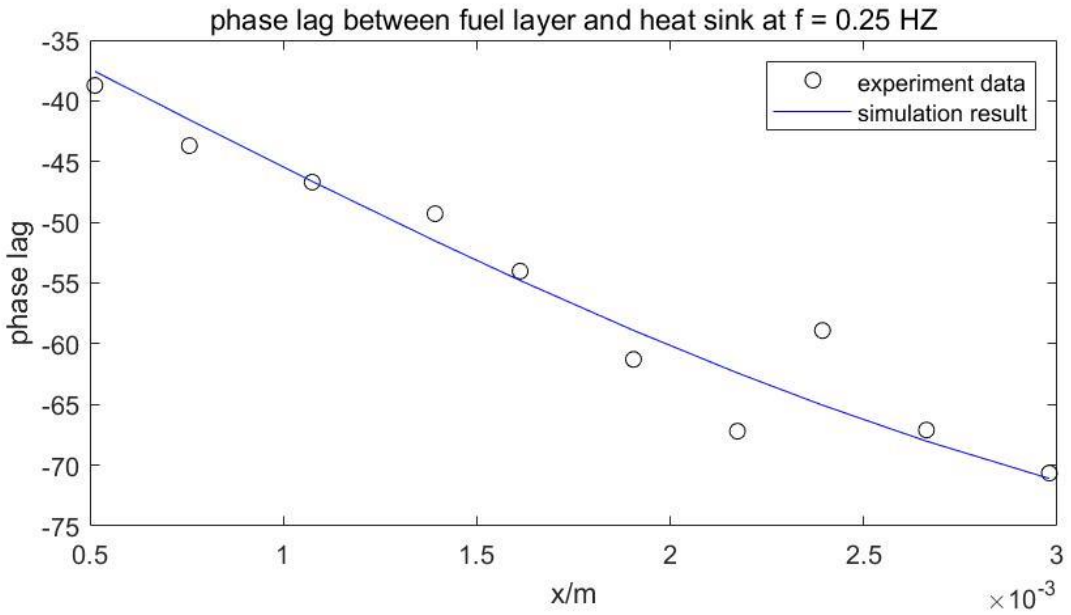

Figure 33. Phase lag comparison at f = 0.25 Hz (value of thermal contact resistance is equal to 2.9214e-05 K/W)

4.3 Solution for the Change of Thermal Contact Resistance

In order to reduce the change of thermal contact resistance between fuel layer and cladding layer, the adjustment of sample fixture is shown as Figure 34. Two fixed components are applied to fix the position of heat sink, and one adjustable clamping component is applied to pressure the fuel layer. The temperature mapping zone is located on this region that is fixed by extra forces. In addition, the holes of heat sink, which is used for the two bolts, are expanded, in order to accommodate the lateral expansion of material. Through these adjustments, the range of thermal contact resistance would be at least smaller than before.

The result of this sample adjustment is shown as Figure 35, Figure 36 & Figure 37. Figure 35 shows the comparison between theoretical prediction and experiment result by using the

thermal contact resistance of curve fitting result under 0.15 Hz in the simulation program. The value of thermal contact resistance is 6.4188e-05 K/W.

Figure 35 shows the comparison between theoretical prediction and experiment result by using the thermal contact resistance of curve fitting result under 0.20 Hz in the simulation program. The value of thermal contact resistance is 4.8166e-05 K/W.

Figure 36 shows the comparison between theoretical prediction and experiment result by using the thermal contact resistance of curve fitting result under 0.25 Hz in the simulation program. The value of thermal contact resistance is 3.8659e-05 K/W.

For these three frequencies, the value of thermal contact resistance is still different, but these three groups of data are the groups that have thermal contact resistance which is close to each other. Excluding these three groups of data, under other frequencies, the change of thermal contact resistance became similarly smaller than before which would indicate the adjustment of the sample works. However, through these adjustments, thermal contact resistance between fuel layer and cladding layer still change, in a small range, along all frequencies. The change of thermal contact resistance makes curve fitting along frequency axis still requires further a solution to be conducted after the experimental adjustment.

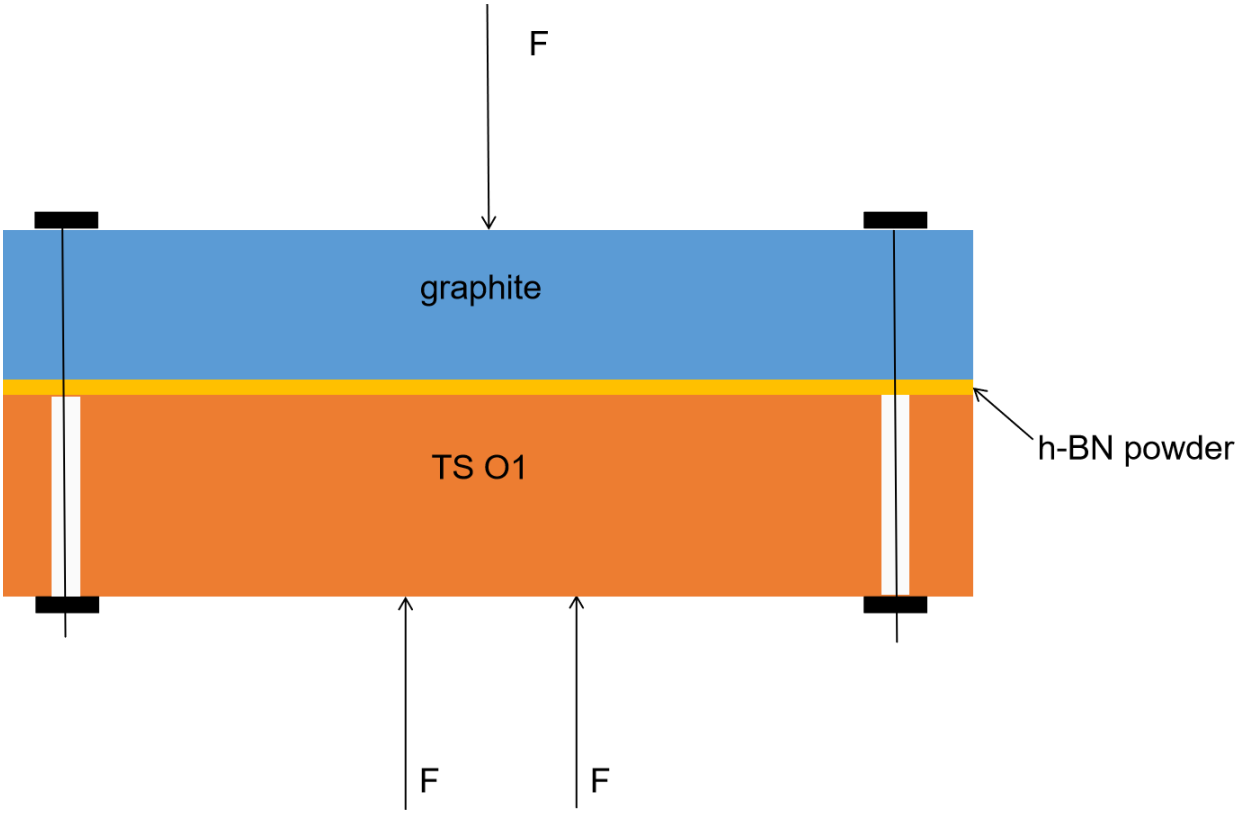

Figure 34. Solution sample model for change of thermal contact resistance

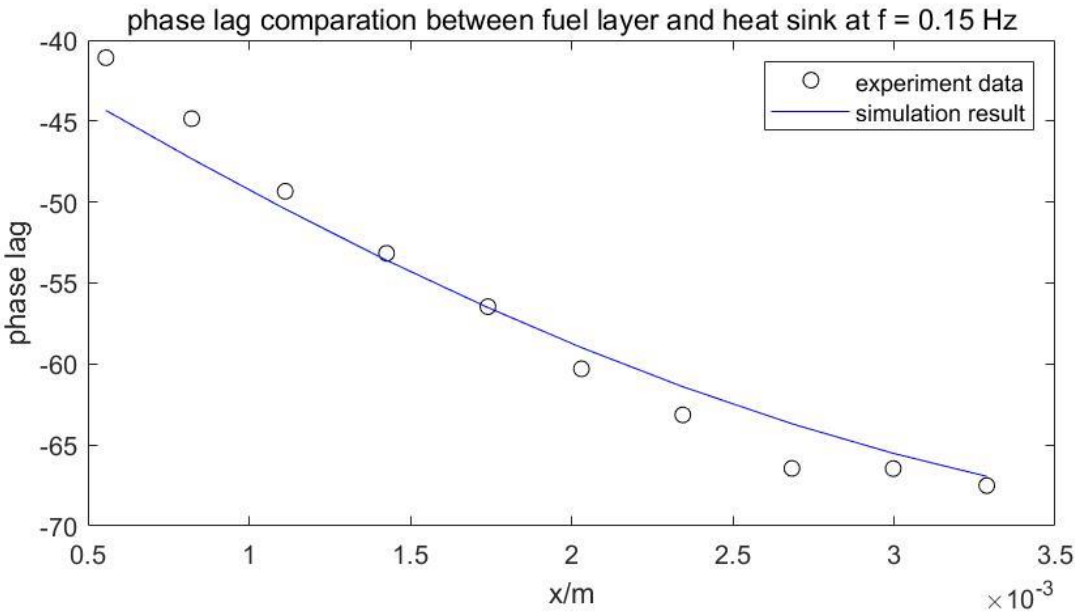

Figure 35. Phase lag comparison at f = 0.15 Hz (value of thermal contact resistance is equal to 6.4188e-05 K/W)

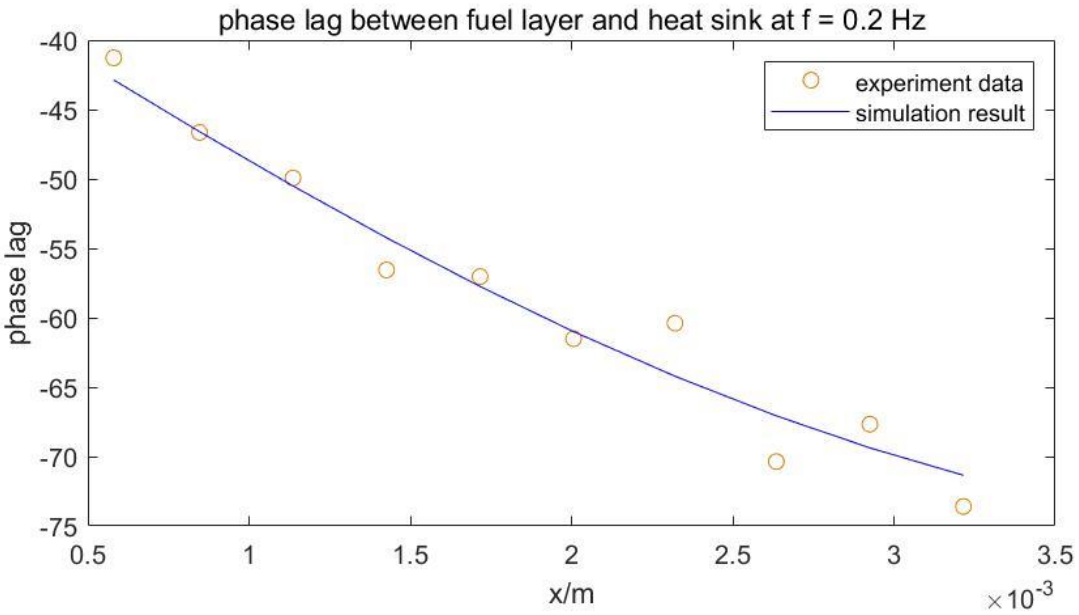

Figure 36. Phase lag comparison at f = 0.20 Hz (value of thermal contact resistance is equal to 4.8166e-05 K/W)

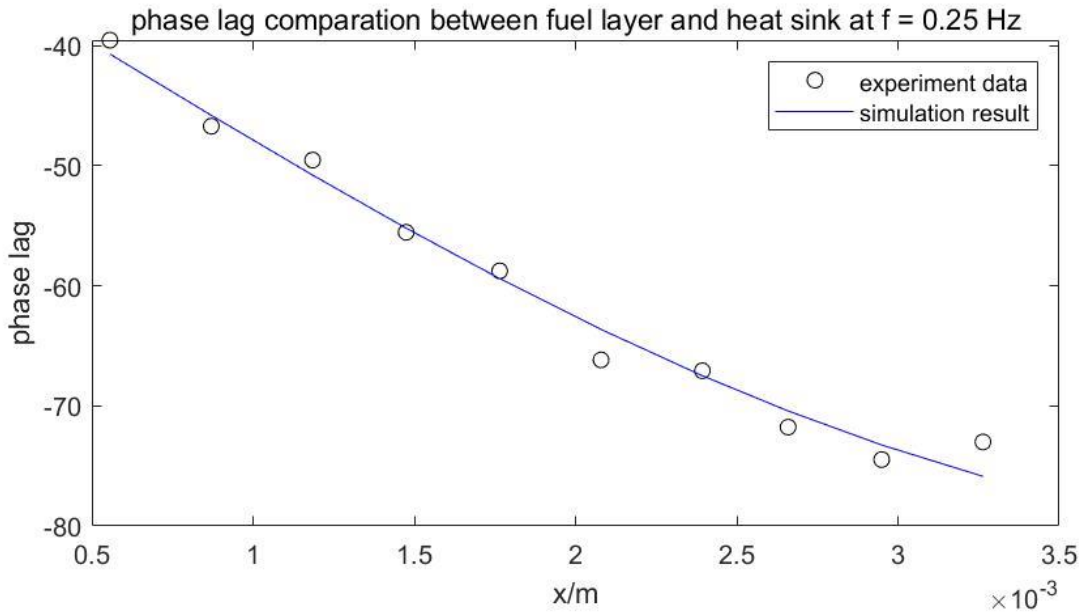

Figure 37. Phase lag comparison at f = 0.25 Hz (value of thermal contact resistance is equal to 3.8659e-05 K/W)

4.4 Applicability of Measurement Method

In the experiment, the extraction of thermal diffusivity of the fuel layer cannot be done using only temperature phase lag as function of frequency due to the change of thermal contact resistance between fuel layer and cladding layer. However, the applicability of measurement method can still be tested by using temperature phase lag as a function of both frequency and spatial variation.

In the experiment, phase lag data under f = 0.10, 0.15, 0.20, 0.25, 0.30, 0.35 Hz are collected at the same measuring point on heat sink among all these frequencies. The experiment results are shown in the yellow line of Figure 38, which contain the experiment data under f = 0.10, 0.15, 0.20, 0.25, 0.30, 0.35 Hz, and the blue line is the theoretical prediction of simulation program

under these frequencies. For the simulation program, the thermal contact resistance under f = 0.2 Hz is applied, and the thermal contact resistance and sensitivity of this measuring point under all frequencies are shown in Table 2.

Based on the definition of sensitivity in the experiment, if the thermal contact resistance (Rth) changes 1%, the phase lag will also change 1% of sensitivity of Rth on that measuring point. For example, at f = 0.15 Hz, the sensitivity of Rth is -6.306°. Under this frequency, if the thermal contact resistance has become 10% larger, the phase lag of all measuring point will decrease 0.6305° under this frequency. In Table 2, phase prediction change means the calculation result of phase lag change because of change of thermal contact resistance, and actual phase change is the data difference of phase lag between experiment result and theoretical prediction. After removing the change of phase layer, caused by the change of thermal contact resistance, based on the sensitivity analysis result, the experiment data is shown as the red line in Figure 38.

By comparing the experiment data after processing and the simulating result, expect at 0.10 Hz, these two groups of data fit relatively well. This result means that if the actual thermal contact resistance is known under every frequency or it is constant in the experiment, there is a possibility that the thermal diffusivity of fuel layer can be measured through this method.

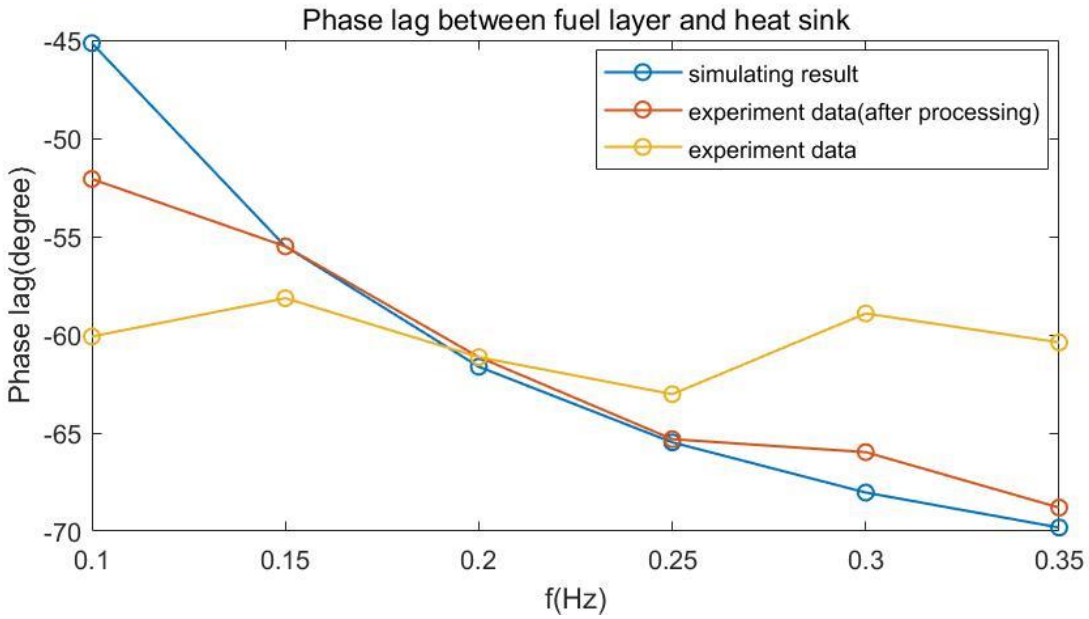

Figure 38. Phase lag comparison under f = 0.10, 0.15, 0.2, 0.25, 0.30, 0.35 Hz (red line is experiment result and blue line is simulation result)

Table 2. Comparison of different frequency

Frequency/ Hz	Thermal contact resistance/ K/W	Sensitivity of Rth	thickness change/ %	phase change prediction	actual phase change
0.10	1.1791e-04	-5.548°	144.80	-8.02°	-15°
0.15	6.4188e-05	-7.949°	33.26	-2.64°	-2.74°
0.20	4.8166e-05 (used for simulation)	-9.982°	0.00	0°	0.36°
0.25	3.8659e-05	-11.63°	-19.74	2.29°	2.29°
0.30	2.1819e-05	-12.9°	-54.70	7.06°	8.92°
0.35	1.8932e-05	-13.86°	-60.68	8.41°	9.2°

4.5 Conclusion

In this study, a plane 1-D model for a multi-layered system under harmonic Joule heating was developed for the thermal wave method. Sensitivity analysis based on the theoretical model showed the effect of all property, geometry and operation parameters. In the validation experiment, the thermal contact resistance between the fuel layer and the cladding layer has shown a strong influence on the measurement of thermal diffusivity of fuel layer. In addition, the actual value of thermal contact resistance was found to change under different heating frequencies, which makes

the measurement of thermal diffusivity of the fuel layer difficult. The adjustments of sample fixture reduced the magnitude of change of thermal contact resistance under different frequencies, but it doesn't fix them as constant. However, by applying the sensitivity analysis result to the comparison of experiment data and simulation result, the method of measuring thermal diffusivity of fuel layer by thermal wave method based on Green function is found to be feasible, as long as the actual value of thermal contact resistance between fuel layer and cladding layer can be measured, or kept constant.

In addition, if the same method is applied in the 3-layer cylinder, and the cladding layer is filled with liquid material, then it can be surmised that the thermal contact resistance can be minimized for the measurement of thermal diffusivity of fuel layer. This study establishes a theoretical and experimental foundation for future application of the method.

Bibliography

[1] Hua Z, Ban H. Thermal diffusivity measurement of focused-ion-beam fabricated sample using photothermal reflectance technique[J]. Review of Scientific Instruments, 2017, 88(5): 054901.

[2] Bauer T H, Holland J W. In-pile measurement of the thermal conductivity of irradiated metallic fuel[J]. Transactions of the American Nuclear Society;(United States), 1992, 65(CONF-920606--).

[3] Horne K, Ban H, Mandelis A, et al. Photothermal radiometry measurement of thermophysical property change of an ion-irradiated sample[J]. Materials Science and Engineering: B, 2012, 177(2): 164-167.

[4] Parker W J, Jenkins R J, Butler C P, et al. Flash method of determining thermal diffusivity, heat capacity, and thermal conductivity[J]. Journal of applied physics, 1961, 32(9): 1679-1684.

[5] Healy J J, De Groot J J, Kestin J. The theory of the transient hot-wire method for measuring thermal conductivity[J]. Physica B+ c, 1976, 82(2): 392-408.

[6] Li C, Su C H, Lehoczky S L, et al. Thermophysical properties of liquid Te: Density, electrical conductivity, and viscosity[J]. Journal of applied physics, 2005, 97(8): 083513.

[7] Rempe J L, Knudson D L, Condie K G, et al. New sensors for the advanced test reactor national scientific user facility[J]. IEEE Transactions on Nuclear Science, 2010, 57(5): 2653-2661.

[8] BuSSe G, Wu D, Karpen W. Thermal wave imaging with phase sensitive modulated thermography[J]. Journal of Applied Physics, 1992, 71(8): 3962-3965.

[9] Opsal J, Rosencwaig A, Willenborg D L. Thermal-wave detection and thin-film thickness measurements with laser beam deflection[J]. Applied Optics, 1983, 22(20): 3169-3176.

[10] Wong Y H, Thomas R L, Pouch J J. Subsurface structures of solids by scanning photoacoustic microscopy[J]. Applied Physics Letters, 1979, 35(5): 368-369.

[11] Murphy J C, Aamodt L C. Photothermal spectroscopy using optical beam probing: mirage effect[J]. Journal of Applied Physics, 1980, 51(9): 4580-4588.

[12] Busse G, Rosencwaig A. Subsurface imaging with photoacoustics[J]. Applied Physics Letters, 1980, 36(10): 815-816.

[13] Busse G, Renk K F. Stereoscopic depth analysis by thermal wave transmission for nondestructive evaluation[J]. Applied physics letters, 1983, 42(4): 366-368.

[14] Ploss B, Emmerich R, Bauer S. Thermal wave probing of pyroelectric distributions in the surface region of ferroelectric materials: A new method for the analysis[J]. Journal of applied physics, 1992, 72(11): 5363-5370.

[15] Bhusari D M, Teng C W, Chen K H, et al. Traveling wave method for measurement of thermal conductivity of thin films[J]. Review of scientific instruments, 1997, 68(11): 4180-4183.

[16] Weisstein E W. Green's function[J]. 2004.

[17] Bhaskaran-Nair K, Kowalski K, Shelton W A. Coupled cluster Green function: Model involving single and double excitations[J]. The Journal of chemical physics, 2016, 144(14): 144101.

[18] Dahlen N E, Stan A, van Leeuwen R. Nonequilibrium Green function theory for excitation and transport in atoms and molecules[C]//Journal of Physics: Conference Series. IOP Publishing, 2006, 35(1): 324.

[19] Abrikosov A A, Gor'Kov L P. Superconducting alloys at finite temperatures[J]. Sov. Phys. JETP, 1959, 9(1): 220-221.